NORWEGIAN SCHOOL OF SPORT SCIENCES

Max Ullrich

MACS – project thesis

The myonuclear specific DNA methylome after resistance training in humans.

Master thesis in Sport Science

Department of Physical Performance

Norwegian School of Sport Sciences, 2023

Preface

I stand at the culmination of this remarkable journey, filled with gratitude and a deep sense of accomplishment. Pursuing a graduate degree is akin to embarking on an intense, often challenging adventure filled with intellectual exploration, endless curiosity, and a quest for knowledge. It is a voyage where one is never alone, and I have been fortunate to share my journey with a multitude of exceptional individuals to whom I owe my sincere thanks.

Firstly, I want to express my deepest appreciation to my primary supervisor, Adam P. Sharples. Your unwavering guidance, encouragement, and expertise in navigating through the nuances of our field have been instrumental in shaping my work and me as a researcher. Your meticulous review of my manuscript and thoughtful advice during planning and analysis have been invaluable, and I am grateful for your dedication and commitment to my project.

I am profoundly indebted to Daniel C. Turner, whose significant contributions made this project feasible. Your guidance at each stage of this project has been remarkable and has undoubtedly shaped the success of this work. Your support has made a significant impact on my research journey, and I cannot thank you enough.

I also want to extend my heartfelt thanks to our diligent bachelor students – Benjamin T. Strømsvold, Emil Carlsen, Ingrid Hansen, Manuel Alfaro, and Marie Matre. Your invaluable assistance in the resistance training intervention and physiological testing formed the bedrock of this study. I have been privileged to work alongside such a committed and talented team.

To our participants, your contribution has been the cornerstone of this research. Without your time, commitment, and effort, this work would not have been possible. I am immensely grateful for your participation.

On a personal note, I am eternally grateful to my girlfriend, Marlene J. Myrbråten, for her ceaseless support, understanding, and resilience. Your strength in dealing with my stress, and your unwavering belief in me, were the pillars I leaned on throughout this journey. Thank you for being my rock.

Finally, my family and friends deserve a special mention for their unwavering support and understanding. Your patience, as I delved deep into my research, often unable to participate in our social life, means more to me than I can express. Your warmth and acceptance as I now re-enter 'the real world' fill me with anticipation and gratitude.

I step forward with the knowledge that this milestone would not have been achieved without your support and faith. To everyone who has been part of this journey, I extend my deepest thanks.

Abstract

Background: Resistance training (RT) is known to induce significant adaptations in skeletal muscle, but the underlying molecular mechanisms driving these adaptations, particularly the role of epigenetic changes, remains incomplete. Using Magnetically Activated Cell Sorting (MACS) with the myonuclei specific marker Pericentriolar material 1 (PCM1), we provide the first cell population specific epigenomic information in human skeletal muscle before and after adaptation to RT. **Methods:** Nine previously strength un-trained participants underwent 7 weeks of supervised progressive high volume resistance training. Genomic DNA was isolated from MACS purified myonuclei (MYO) and from all nuclei within whole skeletal muscle tissue that included myonuclei and interstitial nuclei (MYO+INT) from the vastus lateralis of the non-dominant leg before (baseline) and after (post) the intervention. Using Illumina EPIC arrays, we compared the effect of RT on the methylome of MYO vs. MYO+INT. **Results:** All participants significantly increased their lean mass by 6.0±2.6% equaling 3.3±1.5kg ($p<0.0005$) following RT. A total of 223,352 differentially methylated probes (DMPs) in untrained muscle, and 232,035 DMPs in trained muscle were identified in the MYO vs. MYO+INT cell nuclei populations (FDR < 0.05). Additionally, post vs. baseline comparison identified 27,599 DMPs in MYO and 20,543 DMPs in MYO+INT cell populations following RT ($p<0.05$). Only 1.9%/901 DMPs overlapped between MYO and MYO+INT cell nuclei populations following RT, of which only 548 DMPs observed the same directionality of differential methylation. Although both cell populations were hypomethylated across all DMPs following RT, when focusing specifically on DMPs located in CpG islands within gene promoter regions, the MYO cell population had a predominantly hypermethylated profile post RT (70.7%/1,789 DMPs hypermethylated) while MYO+INT had a predominantly hypomethylated profile following RT (54.7%/1,032 DMPs hypomethylated). Utilizing over-representation analysis (ORA) we identified 39 significant pathways in MYO+INT and 52 significant pathways in MYO ($p < 0.05$), with 14 pathways significantly over-represented in both cell nuclei populations following RT. Six of the shared pathways (Lysine degradation, Cell cycle, Oxytocin signaling pathway, Endocrine and other factor-regulated calcium reabsorption, and Carbohydrate digestion and absorption) observed opposite directionality of differential methylation following RT. Interestingly, the canonical Wnt/β-catenin signaling pathway

observed a hypomethylation in MYO+INT and hypermethylation in MYO cell populations following RT, indicating a differential role for Wnt pathway genes in human myonuclei and interstitial cells. Additionally, ORA identified over-representation of Leukocyte transendothelial migration as well as fibroadipogenic progenitor- and endothelial cell specific gene sets exclusively in the MYO+INT cell population. **Conclusion:** Taken together, these data suggest differential methylation consistent with cell population specific adaptations to RT. Additionally, the present study highlights that interpretation of whole skeletal muscle tissue methylation profiles should begin to take account of cell nuclei specific alterations and that the differences between myonuclear and interstitial DNA methylation profiles resulting from varying myonuclear and interstitial cell proportions should be considered.

Table of Contents

List of abbreviations

4E-BP1 - Eukaryotic initiation factor 4E-binding protein 1

ADP - Adenosine Diphosphate

Akt - Protein kinase B

AMPK - AMP-activated protein kinase

ATP - Adenosine Triphosphate

AXIN1 - Axis Inhibition Protein 1

BANP - BTG3 Associated Nuclear Protein

BRAF - B-Raf Proto-Oncogene

CADM4 - Cell Adhesion Molecule 4

Ca2+ - Calcium Ion

CCDC88C - Coiled-Coil Domain Containing 88C

CCND1 - Cyclin D1

CHD8 - Chromodomain Helicase DNA Binding Protein 8

CpG - Cytosine-Phosphodiester Bond-Guanine

CSA - Cross Sectional Area

CSNK2B - Casein Kinase 2 Beta

CTBP1 - C-Terminal Binding Protein 1

CXCL2 - C-X-C Motif Chemokine Ligand 2

DEG - Differentially Expressed Gene

DHPR - Dihydropyridine Receptor

DMG - Differentially Methylated Gene

DMP - Differentially Methylated Probe

DOMS - Delayed Onset Muscle Soreness

DVL3 - Dishevelled Segment Polarity Protein 3

eEF2 - Eukaryotic Elongation Factor 2

eIF4E - Eukaryotic Translation Initiation Factor 4E

EWAS - Epigenome-Wide Association Studies

FACS - Fluorescence Activated Cell Sorting

FAP - Fibroadipogenic Progenitor Cells

FAK - Focal Adhesion Kinase

FOXO - Forkhead Box O

FRAT2 - FRAT Regulator of WNT Signaling Pathway 2

FZD8 - Frizzled Class Receptor 8

FUBP1 - Far Upstream Element Binding Protein 1

GH - Growth Hormone

GPR125 (ADGRA3) - Adhesion G Protein-Coupled Receptor A3

GSK3β - Glycogen Synthase Kinase 3-Beta

GTPase - Guanosine Triphosphate Hydrolizing Enzyme

HIST1H2BJ - H2B Clustered Histone 11

HPCAL1 - Hippocalcin Like 1

IGF-1 - Insulin-Like Growth Factor 1

IGF2 - Insulin-Like Growth Factor 2

INT - Interstitial Cell Nuclei

JOSD2 - Josephin Domain Containing 2

KEGG - Kyoto Encyclopedia of Genes and Genomes

LGR6 - Leucine Rich Repeat Containing G Protein-Coupled Receptor 6

LKB1 (STK11) - Liver Kinase B1/Serine/Threonine Kinase 11

MACS - Magnetically Activated Cell Sorting

MAD1L1 - Mitotic Arrest Deficient 1 Like 1

MAFbx - Muscle Atrophy F-Box

MAPK - Mitogen Activated Protein Kinase

MeDEG - Differentially Methylated Differentially Expressed Gene

MPS - Muscle Protein Synthesis

MPB - Muscle Protein Breakdown

mRNA - Messenger RNA

mTORC1 - Mammalian Target of Rapamycin Complex 1

MuRF1 - Muscle RING Finger 1

MyHC1 - Myosin Heavy Chain 1

MYO - Myonuclei

NAD+/NADH - Nicotinamide Adenine Dinucleotide + Hydrogen

NBN - Nibrin

NF-κβ - Nuclear Factor Kappa Beta

NRF1 - Nuclear Respiratory Factor 1

ORA - Over-Representation Analysis

PAX7 - Paired Box 7

PCA - Principal Component Analysis

PCM1 - Pericentriolar Material 1

PGC-1α - Peroxisome Proliferator-Activated Receptor-Gamma Coactivator

pi - Inorganic Phosphate

PI3K - Phosphoinositide 3-Kinase

POLR1C - RNA Polymerase I and III Subunit 3

RF - M. Rectus Femoris

RPE - Rate of Perceived Exertion

RRBS - Reduced Representation Bisulfite Sequencing

RT – Resistance Training

RYR - Ryanodine Receptor

SC - Satellite Cell

SERCA - Sarcoendoplasmic Reticulum Calcium ATPase

SkM – Skeletal Muscle

SMAD9 - SMAD Family Member 9

SR – Sarcoplasmic Reticulum

STRADA - STE20 Related Adaptor Alpha

TET (TET1, TET2, TET3) - Ten-Eleven Translocation Enzymes

TGF-β - Transforming Growth Factor Beta

TNF-a - Tumor Necrosis Factor Alpha

TNRC18 - Trinucleotide Repeat Containing 18

TSC - Tuberous Sclerosis Complex

TSC2 - Tuberous Sclerosis Complex 2

TSS - Transcriptional Start Site

UBR5 - Ubiquitin Protein Ligase E3 Component N-Recognition 5

VL - M. Vastus Lateralis

WNT1 - Wnt Family Member 1

Wnt - Wingless-Related Integration Site

1.0 Structure of thesis

Decades of research into skeletal muscle (SkM) physiology has provided great insight on the structural and functional components of this complex tissue that is responsible for generating force and movement. With the advent of “omics” technology, it is possible to investigate minute molecular features within the complex SkM tissue niche in response to internal and external stimuli that ultimately results in skeletal muscle’s uniquely remarkable plasticity. Indeed, SkM is the body’s most abundant and adaptive tissue, readily adapting to external stimuli, like resistance and endurance exercise, leading to changes in composition, size, force generating capacity, and metabolism. These tissues, such as SkM, are made up of multiple cell populations that all share the same genome, however, it is their specific gene expression and gene repression, through mechanisms such as epigenetics, that determines cell population specific characteristics. Epigenetics is the study of how environmental factors, including exercise, coordinate modifications to our inherited gene sequence, which in turn regulates their rate of expression. Using epigenomics, we aim to ascertain which genes are regulated via epigenetic modifications, in response to chronic resistance training (RT), that subsequently leads to increases in strength and hypertrophy. To deconvolute the precise regulation of gene expression, it is important to consider the multicellular composition of the SkM tissue niche, with the latest studies identifying as many as 12 unique cell populations in SkM tissue that possess unique gene expression profiles (Soule, et al., 2023). To our knowledge, the present study provides the first ever genome-wide DNA methylation analysis across different cell populations within human skeletal muscle. Specifically, DNA methylation profiles of muscle cell nuclei (termed myonuclei) all nuclei within SkM tissue (composed of interstitial cell nuclei plus myonuclei derived from the whole tissue homogenate) were assessed before and after 7 weeks of RT in previously strength untrained males.

This thesis will first provide a general overview of complex SkM physiology, structure, and function. All major adaptations to internal and external stimuli are ultimately driven by changes in gene expression and protein content (Jaenisch & Bird, 2003). Therefore, the next section covers the process of gene transcription, and how these processes are regulated via epigenetic modifications to DNA, followed by a brief overview of cell specific epigenetic and gene expression profiles. Finally, the importance and

associated difficulties of distinguishing cell populations for interrogating mechanistic insight into molecular regulation of SkM is introduced, and the aims and hypothesis of this study are presented.

The second chapter of this thesis covers the in-depth methods employed throughout this study, from the ethics, study design and anthropological measures, to methods related to the isolation and subsequent epigenetic analysis of myonuclear DNA.

The next section of this thesis encompassing the results, discussion, and conclusion, form the preliminary manuscript that will be submitted to a peer-reviewed scientific journal. The final manuscript will encompass a more concise introduction and methods already presented in this thesis (in line with *AJP-Cell Physiology* guidelines as the peer reviewed journal targeted for submission) including analyses and results outside the scope and time constraint of the present thesis.

2.0 Background and theory

Skeletal muscle (SkM) makes up the majority of all human body tissue, accounting for ~40% of total body weight in healthy untrained males (Janssen, Heymsfield, Wang, & Ross, 2000). SkM tissue allows, amongst other things; normal body posture, breathing, voluntary movement, locomotion, metabolism, and maintenance of body temperature (Loreti & Sacco, 2022). SkM tissue is composed of highly organized, complex interactions of multiple structures and cell types. The muscle is formed by multiple fascicles, that themselves are comprised of multinucleated muscle fibers. Each level of organization itself is surrounded by connective tissue membranes often referred to as fascia, where the epimysium surrounds the entire muscle, the perimysium encompasses each fascicle, and the endomysium separates the single fibers (Purslow, 2010). SkM is highly vascularized and innervated, which allows it to function as a biomechanical device, that produces repeated contraction-relaxation cycles that ultimately result in force production and movement (Mukund & Subramaniam, 2019). As previously mentioned, SkM his highly adaptive and can readily respond to intrinsic and extrinsic stimuli by increasing and decreasing in size, changing mechanical and metabolic properties etc. (Loreti & Sacco, 2022; Mukund & Subramaniam, 2019; Egan & Sharples, 2023). These adaptations require a synchronization of all the structures

and cell populations that comprise the complex SkM tissue, such as: satellite cells, fibroblasts, fibroadipogenic progenitors (FAPs), endothelial cells, adipocytes, immune cells, and smooth muscle (Soule, et al., 2023). The following section will cover the components and ultrastructure of multinucleated SkM cells, followed by an overview of cell population-specific adaptations to RT.

2.1 Skeletal muscle ultrastructure and function

Each SkM fibre is comprised by an elongated cylindrical multinucleated cell, containing multiple myofibrils that are supported by the cytoskeletal network (Figure 1). The SkM is encapsulated by the sarcolemma that propagates the action-potential from the neuromuscular junction (NMJ), trough transverse-tubules (t-tubules) that perturbates in between the muscle fibrils, to the triad junction connecting to the sarcoplasmic reticulum (SR). When the action-potential depolarizes the dihydropyridine receptor (DHPR), a voltage-gated calcium ion channel that through ryanodine receptors (RYR) causes the rapid release of Ca^{2+} from the SR into the cytoplasm and reuptake back into SR through the sarcoendoplasmic reticulum calcium ATPase (SERCA) pump. As seen in figure 1, each SkM fiber has multiple t-tubules and an extensive network of SR that leads to rapid release and reuptake of Ca^{2+} caused by action potentials that are

propagated from motor neurons to the sarcolemma of individual SkM fibers (Mukund & Subramaniam, 2019).

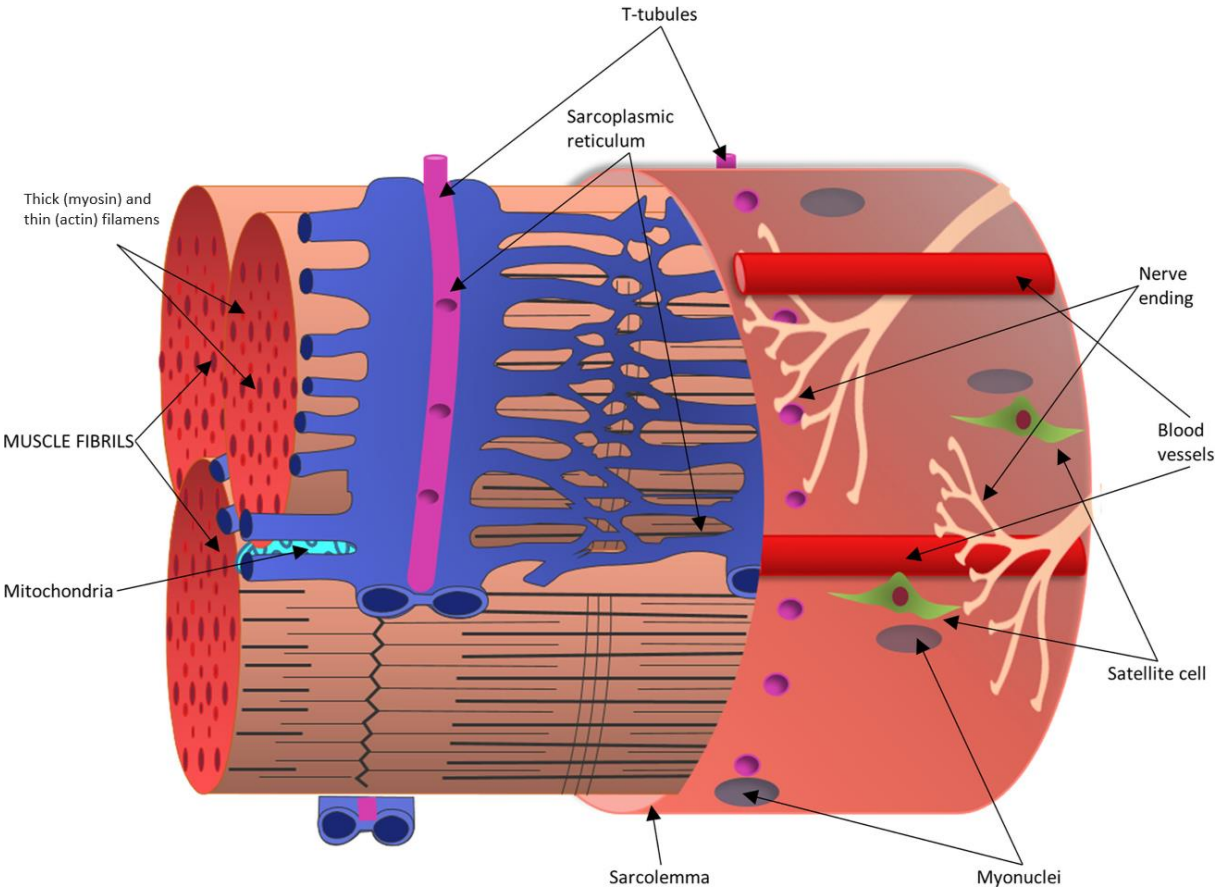

Figure 1. Schematic representation of a single mature skeletal muscle fiber image adapted from Mukund & Subramaniam (2019).

The well-established sliding filament model of force production/muscle contraction was introduced by Huxley et al. (1957), that proposed a mechanism of muscle contraction through force-generating interactions between myofilaments (myosin and actin) (Figure 2A.). Myosin filaments use energy from ATP to perform a “power-stroke” that causes movement along the actin filaments, thus causing the sarcomeres to shorten (Huxley, 1957; Mukund & Subramaniam, 2019). As previously mentioned, the Ca^{2+} release from SR causes conformational changes to troponin C, revealing myosin binding sites on the actin filament, causing myosin to initiate the cross-bridge cycle that leads to shortening of the sarcomere. Through this inverted mechanism, reuptake of Ca^{2+} into SR causes the release of myosin and subsequent relaxation/lengthening of the sarcomere. As seen in Figure 2, each myofibril is surrounded by a complex mesh

of cytoskeletal proteins such as dystrophin, and α-actin assembled into F-actin filaments, that support the structure and function of the myofibrils through stretch-shortening cycles. These cytoskeletal proteins also propagate force from the z-disk laterally to the sarcolemma, through costameres (Figure 2B.) and finally transfer the contractile force to the extracellular matrix (ECM) through the dystrophin-associated protein complex (Mukund & Subramaniam, 2019). This contractile force is then propagated through highly collagenous connective tissue across the endomysium, perimysium and epimysium, finally inserting into the bone via the tendons.

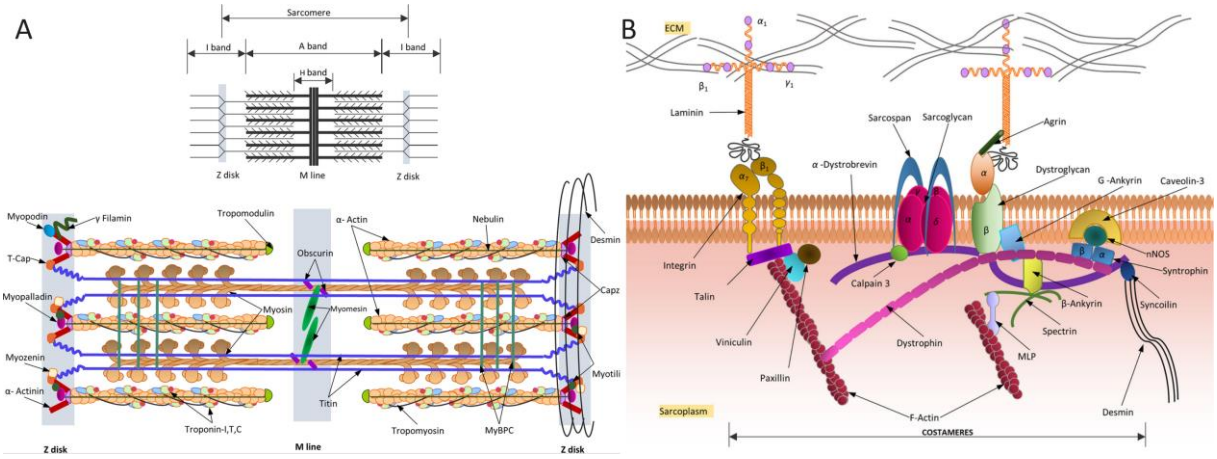

Figure 2. A: Illustration of the sarcomere, showing the organization and location of the major sarcomeric proteins. B: A representation of main proteins of costameres that provide a strong mechanical link between the intracellular cytoskeleton and the extracellular matrix image adapted from Mukund & Subramaniam (2019).

2.2 Muscle hypertrophy and the regulation of gene expression

Transient and repeated homeostatic perturbations are central to why and how cells, tissues and organs adapts to exercise (Egan & Sharples, 2023). In the context of this thesis, we will focus on the homeostatic perturbations caused by resistance exercise in only SkM. These homeostatic perturbations induce acute responses that activate compensatory mechanisms, leading to re-establishment of homeostasis. Chronically, these compensatory mechanisms adapt to better withstand similar future perturbations. The mechanistic basis leading to the long-term adaptations is still not completely understood. However, the leading consensus is centered on a complex model consisting of a series of sequential and overlapping steps, from the onset of exercise stimulus to a change in enzyme activity, mRNA expression, and protein abundance. This leads to a shift in the ratio between synthesis and breakdown of

proteins, leading to functional, structural, and physiological adaptations following exercise stimuli (Mukund & Subramaniam, 2019; Egan & Sharples, 2023).

Resistance exercise generates mechanical and metabolic signals within SkM, which activate intracellular signaling pathways. The acute exercise stimulus induces several perturbations including, electrolyte imbalance, muscle tissue and cell volume changes, efflux and influx of calcium in the sarcoplasmic reticulum, altered energy states in the ratio between [ATP]/[ADP]/[Pi], altered redox potential [NAD+]/[NADH], declining pH, reduced oxygen partial pressure, increased free radicals, increased intramuscular temperature and intermittent mechanical loading. In addition to these intracellular exercise signals, prolonged exercise will increase energy substrate utilization from both intracellular and extracellular sources. Furthermore, acute exercise stimulus also affects a number of local and systemic variables, including catecholamines, cytokines, and hormones such as testosterone, noradrenaline, TNF-α, GH, and IGF-1. The duration and amplitude of change in any of these signals is highly specific to the intensity, duration, and mode of exercise. In general, these perturbations are sensed by intracellular and/or membrane bound sensor proteins, which are propagated by intracellular signaling pathways through cell signaling cascades. These signaling cascades initiate a series of downstream molecular events, including gene transcription, and protein synthesis (MPS) and protein breakdown (MPB) through modulation of transcription factors and coregulators, translation initiation and elongation factors, and proteolytic regulation, ultimately leading to SkM adaptations (Egan & Sharples, 2023). These signal transduction pathways are often described as linear networks with distinct borders, however there is obvious overlap and interplay between pathways (Egan & Sharples, 2023). Resistance exercise-induced SkM hypertrophy is mediated via the regulation of MPS and MPB where growth occurs when MPS is greater than MPB, resulting in a positive net protein balance. I will therefore briefly describe some of the major pathways pertinent for MPS (e.g. mTORC1) and MPB (ubiquitination and FOXO), AMPK, and Wnt, ultimately related to exercise adaptations in skeletal muscle.

1. mTORC1 Pathway

The mammalian target of rapamycin complex 1 (mTORC1) pathway is a central regulator of muscle protein synthesis (MPS) and plays a crucial role in mediating

resistance exercise-induced muscle hypertrophy (Drummond, et al., 2009). Exercise signals, such as mechanical loading (Hornberger, Chu, Hsuiung, Huang, & Chien, 2006; Spangenburg, Roith, Ward, & Bodine, 2008) and the availability of amino acids (Tipton, Ferrando, Phillips, Doyle Jr, & Wolfe, 1999; Kim & Guan, 2009) activate the mTORC1 pathway. Mechanical loading is sensed by mechanosensitive proteins, like integrins and focal adhesion kinase (FAK), which initiate signaling cascades that eventually converge on mTORC1 activation (Flück, Carson, Gordon, Ziemiecki, & Booth, 1999; Crossland, et al., 2013). A key upstream regulator of mTORC1 is the serine/threonine kinase Akt/PKB (Bodine, et al., 2001). Akt is activated by phosphoinositide 3-kinase (PI3K) in response to growth factors, such as insulin-like growth factor 1 (IGF-1) (Sandri, 2008). Upon activation, Akt phosphorylates and inhibits the tuberous sclerosis complex (TSC), allowing mTORC1 activation by the small GTPase Rheb (Li, Inoki, & Guan, 2004). Additionally, mTORC1 can be activated by amino acids through the Rag GTPases and the lysosomal Ragulator protein complex (Egan & Sharples, 2023; Inoki & Guan, 2022; Kim & Guan, 2009; Tipton, Ferrando, Phillips, Doyle Jr, & Wolfe, 1999). Once activated, mTORC1 phosphorylates downstream targets, including the ribosomal protein S6 kinase 1 (S6K1) and the eukaryotic initiation factor 4E-binding protein 1 (4E-BP1), elF4E and eEF2 (Baar & Esser, 1999; Bodine, et al., 2001). The activation of the mTORC1 pathway leads to the modulation of these effector proteins, that ultimately play crucial roles in ribosomal biogenesis and the formation of the translation initiation complex and the subsequent activation of protein synthesis (Figuiredo & McCarthy, 2019; Bodine, et al., 2001; Egan & Sharples, 2023).

2. AMPK Pathway

The AMP-activated protein kinase (AMPK) pathway is primarily associated with cellular energy homeostasis and plays a crucial role in the regulation of metabolic adaptations in response to exercise. As an energy sensor, the AMPK pathway is most often related to aerobic exercise, however it has also been shown to be activated in a volume dependent manner in resistance exercise (Ahtiainen, et al., 2015). During exercise, the increased energy demand leads to a rise in the AMP/ADP and ADP/ATP ratio within muscle cells. This change in cellular energy status is sensed by AMPK, which becomes activated through phosphorylation by its upstream kinase, liver kinase B1

(LKB1/STK11). In addition, the γ-subunit of AMPK is allosterically regulated by competitive binding of AMP/ADP/ATP, which induces conformational changes that promote phosphorylation of AMPK and reduce dephosphorylation. Together, the combination of allosteric activation and phosphorylation of α-Thr172 leads to a >1000-fold increase in AMPK activity (Suter, et al., 2006; Kjøbsted, et al., 2018).

Once activated, AMPK acts on various downstream targets to promote energy-generating processes, to promote energy availability. Acutely, AMPK suppresses glycogen and protein synthesis, while stimulating glucose uptake and lipid metabolism (Egan & Sharples, 2023; Kjøbsted, et al., 2018; Zhao, et al., 2017). In rodents, acute increase in AMPK activity activates AICAR that phosphorylates glycogen synthase (GS), thus reducing glycogen synthesis. However, AICAR also increases glucose uptake, ultimately leading to intracellular increase in glucose-6-phosphate, which overrides the “previous” AMPK-induced inhibition of GS (Kjøbsted, et al., 2018). As previously mentioned, mTORC1 activity is regulated by the tuberous sclerosis complex. By phosphorylating TSC2 at Thr1227 or Ser1345, AMPK increases TSC2’s ability to inhibit mTOR activity. In addition, AMPK can inhibit mTOR by directly phosphorylating mTOR at Thr2446, which inhibits Akt-mediated mTOR activation (Zhao, et al., 2017; Kjøbsted, et al., 2018). Furthermore, AMPK can phosphorylate Raptor, resulting in mTORC1 inhibition. All of which leads to the reduction in protein synthesis (Kjøbsted, et al., 2018). AMPK activation has also been shown to regulate muscle protein degradation, as a means to increase energy availability. This system involves the activity of E3 ubiquitin ligases, which mediate the ubiquitination and degradation of proteins. AMPK directly phosphorylates forkhead box protein O3a (FOXO3a/FOXO3) at multiple sites, which increases the transcription of muscle atrophy F-box (MAFbx) and muscle RING finger 1 (MuRF1) E3 ligases (Kjøbsted, et al., 2018).

Long term, the repeated yet transient activation of AMPK leads to increased metabolic capacity, mainly through PGC-1α and NRF1 control of mitochondrial biogenesis. However, the precise role of AMPK in resistance exercise-induced adaptations remains an area of ongoing investigation (Kjøbsted, et al., 2018) (Egan & Sharples, 2023).

3. Wnt Pathway

Wnt proteins comprise a large family of growth factors related to development and homeostatic processes. The non-canonical Wnt7a pathway regulates satellite cell self-renewal and migration, as well as myofiber size and strength, whereas the canonical Wnt/β-catenin cascade appears to be primarily engaged in the regulation of satellite cell terminal differentiation. The precise mechanism that controls canonical and noncanonical cascades during muscle regeneration is still poorly understood. However, in skeletal muscle, Wnt signaling has been shown to activate the Akt/mTOR pathway aiding in hypertrophic processes. In addition, Wnt pathways have been linked to adult myogenesis, and satellite cell proliferation through the PCP pathway. As a growth regulator, the canonical Wnt/β-catenin pathway has also been implicated in muscle regeneration (Girardi & Le Grand, 2018). Ultimately, Wnt signaling is related to multiple processes and pathways related to skeletal muscle adaptations to resistance exercise, including MAPK signaling, p53 signaling, TGF-β signaling, cell cycle pathway, focal adhesion pathway, proteolysis, cytoskeletal remodeling, and gene transcription (Hatsell, Rowlands, Hiremath, & Cowin, 2003; Girardi & Le Grand, 2018; Kühl, Sheldahl, Park, Miller, & Moon, 2000; Kanehisa & Goto, 2000; Kanehisa M. , 2019; Kanehisa, Furumichi, Sato, Kawashima, & Ishiguro-Watanabe, 2023). A recent study looking at DNA methylation following progressive weighted wheel running in mice, identified Wnt signaling as a differentially regulated pathway in different skeletal muscle cell populations. Interestingly, the Wnt pathway was hypomethylated in myonuclear promoters and hypermethylated in interstitial nuclei promoter regions (Wen, et al., 2021). Thus, implicating Wnt signaling as a key pathway in skeletal muscle cells specifically following a model of resistance training.

Ultimately, the long-term goal of chronic resistance exercise is an increase in strength through an accruement of muscle mass through hypertrophy. Central to muscle hypertrophy following resistance training is the repeated, yet transient increase in muscle protein synthesis, predominantly as a result in the increased abundance of myofibrillar proteins. Cumulatively, through repeated bouts of progressively heavier resistance training over months and years, leading to substantial increase in size of the resistance trained muscle.

2.3 Epigenetic regulation of gene expression

Acute and chronic exercise leads to structural and functional remodeling of skeletal muscle tissue, facilitated by changes in transcription and translation, leading to gradual protein turnover towards a trained phenotype. Following acute exercise, the majority of transcriptional control mechanisms have been shown to be altered in skeletal muscle, including chromatin accessibility, transcription factor activity, protein stability, and intracellular localization of transcriptional regulators (Egan & Sharples, 2023). Transcriptional regulators include stable and persistent epigenetic regulation by DNA methylation and histone acetylation, which make them ideal epigenetic markers. Transcriptional pre- and post-regulators also include RNA-mediated regulation, including micro-RNA, small interfering RNA, small non-coding RNA, long non-coding RNA, however these are outside the scope of this thesis (Egan & Sharples, 2023). As a stable yet reversible regulator of gene expression, epigenetic regulation through DNA methylation will be the major topic of this thesis and as such will be the only epigenetic marker discussed in depth.

2.3.1 Histone modification

Epigenetic regulation of gene expression refers to the reversible modifications to our DNA, without changing the DNA sequence itself. The two most studied epigenetic regulators are histone modification, which mainly affects the accessibility of the chromatin, and DNA methylation which generally inhibits the binding of the transcriptional apparatus. Briefly, histone modification involves the addition or removal of acetyl- (CH3CO) or methyl groups (CH3) to the histone tails, causing the chromatin to pack tighter or looser to the histones, affecting the accessibility of the specific DNA segments (Egan & Sharples, 2023).

2.3.2 DNA methylation

DNA methylation is catalyzed by a group of enzymes known as methyltransferases (DNMTs), which increase DNA methylation (hypermethylation). DNMT 3a and 3b are mainly involved in de novo methylation, while DNMT1 is responsible for maintaining methylation, for example through the cell cycle and DNA replication. Conversely, the removal of methyl groups (hypomethylation) is facilitated by the ten-eleven translocation (TET) enzymes TET1, TET2 and TET3 (Egan & Sharples, 2023). DNA

methylation involves the transfer of a methyl group from S-adenosyl-methionine (SAM) to the 5th carbon of a cytosine (5mC). The cytosine residue within a cytosine-phosphate-guanine (CpG) dinucleotide sequence on the same strand of DNA is the most susceptible target of methylation. Promoter and enhancer region-specific methylation can directly interfere with the binding of the transcription machinery (e.g. transcription factors and RNA-polymerase), and the interaction between transcription factors that require cytosine interaction, thereby largely leading to gene silencing (McGee & Hargreaves, 2019). Conversely, increased methylation that occurs within gene silencer regions is able to increase gene expression (Jayavelu, Jajodia, Mishra, & Hawkins, 2020).

In vertebrate genomes, more than half of all genes contain short, ~1kb, CpG-rich regions known as CpG islands. As 5mC can spontaneously or enzymatically be converted into thymine through deamination, the remaining genome is largely depleted of CpGs. Advancements in genome-wide methylome analysis have identified that the positional relationship between the transcriptional unit and methylation site influences its relationship to gene control. For example, methylation in the immediate genomic vicinity of transcriptional start sites (TSS) blocks transcription initiation, while gene body methylation does not block and might stimulate transcription elongation. The role of de novo methylation of non-CpG island TSS is still under investigation (Jones, 2012). However, hypomethylation especially in CpG island in promoter and/or enhancer regions is generally associated with increased gene expression, while the converse relationship likely occurs with hypomethylation in silencing regions (Egan & Sharples, 2023). Enhancer regions are mostly CpG-poor regions situated at variable distances from promoters, and are central in the control of gene expression during development and normal cell function. Within a given cell population, the methylation of CpG sites within enhancers has been shown to be dynamically hypo- and hypermethylated, making them an interesting target for methylome analysis in relation to regulation of gene expression. For example, glucocorticoid receptor binding to distal regulatory regions showed that the hypomethylation of CpGs could activate the enhancer in the presence of the receptor. Interestingly, the methylation of insulators might be of particular interest, as these elements block the enhancer-promoter interaction, thus affecting gene expression. Transcription factor binding can be strongly influenced by methylation of CpG sites within their recognition sequences, pointing to a cause-and-

effect relationship between TSS related hypermethylation of CpGs and repression of gene expression. However, since transcription factors can bind strongly to methylated DNA sequences, the cell population and gene specific role of DNA methylation is still under investigation (Jones, 2012).

2.4 The cellular heterogeneity issue in Epigenome-Wide Association Studies (EWAS)

As previously mentioned, skeletal muscle is a complex heterogenous tissue consisting of multinucleated muscle fibers, immune cells, endothelial cells, satellite cells, FAPs and other mononucleated cell populations (Mukund & Subramaniam, 2019; Rubenstein, et al., 2020). Previous studies in human blood, found that global DNA methylation differed between whole blood and the individual cell populations, and between the major cell populations like B cells, T cells, and Monocytes/Granulocytes/Neutrophiles/Eosinophils (Reinius, et al., 2012). To our knowledge, single cell/single nuclear epigenomic profiling has not previously been performed in human skeletal muscle. However, recent studies in single cell transcriptomics have shown as many as 11 mononuclear cell populations in human skeletal muscle with distinct gene expression profiles (Rubenstein, et al., 2020), while single nuclear transcriptomics identified 12 mono- and multinucleated cell populations (Soule, et al., 2023). Significant epigenomic differences have been observed between myonuclei and interstitial cells (Wen, et al., 2021; Von Walden, et al., 2020), and between slow- and fast phenotype myonuclei and whole muscle tissue (Bengtsen, et al., 2021). As epigenomic profiling by sequencing and arrays provide an average of the entire sample, cellular heterogeneity in complex tissues like skeletal muscle pose an issue in EWAS. In addition, resistance exercise has been shown to cause changes in myonuclear density (Sharples & Turner, 2023; Bagley, Denes, McCarthy, Wang, & Murach, 2023; Bruusgaard, Johansen, Egner, Rana, & Gundersen, 2010; Bjørnsen, et al., 2019) and immune cell infiltration (Rigamonti, Zordan, Sciorai, Rovere-Querini, & Brunelli, 2014; Paulsen, et al., 2010; Paulsen, Mikkelsen, Raastad, & Peake, 2012), potentially causing substantial changes in cell-population proportions, further affecting whole tissue epigenomics. In this section, two potential sources of cell population proportion shift following chronic RT will be discussed. Namely, myonuclear addition and immune cell infiltration.

2.4.1 Myonuclear addition

As skeletal muscle fibers hypertrophy, myonuclei are added through the process of satellite cell fusion. Although variable, the number of nuclei seems to be relatively proportional to cytoplasmic volume, a concept referred to myonuclear domain. Specifically in slow twitch fibers this correlation seems particularly strong, while less so in fast twitch fibers (Gundersen, 2016). However, myonuclear domain can change rapidly during periods of muscle fiber hypertrophy or atrophy (Bagley, Denes, McCarthy, Wang, & Murach, 2023). Myonuclear addition has been largely observed in a variety of hypertrophic conditions, while it does not seem to be strictly necessary to facilitate short-term hypertrophy. However, in longer training periods such as >8 weeks, the inhibition of SC fusion and thus myonuclear accretions may potentially blunt the muscle fibers ability to adapt to chronic resistance exercise, specifically in larger muscle fibers (Sharples & Turner, Skeletal Muscle Memory, 2023). The current literature in humans is somewhat ambiguous to which degree myonuclei from earlier episodes of hypertrophy are retained, and for how long, or if myonuclei are even increased following traditional RT. Current evidence from animal studies allows for the possibility that accrued myonuclei earlier in life may at least partially be retained, thereby serve to promote muscle tissue regrowth later in life (Snijders, et al., 2020). However, emerging evidence suggests that myonuclei are lost after a prolonged period of atrophy (Bagley, Denes, McCarthy, Wang, & Murach, 2023).

The time course of myonuclear accretion relative to other nuclei in skeletal muscle tissue is the main issue when performing DNA methylation analysis. Several studies have shown that myonuclear accretion supersedes fiber CSA increase, thereby increasing the myonuclei to other nuclei proportion (Bruusgaard, Johansen, Egner, Rana, & Gundersen, 2010; Bjørnsen, et al., 2019; Aloisi, Mussini, & Schiffino, 1973). Bruusgard et al. (2010) observed a 35% increase in fiber CSA with a concurrent 54% increase in myonuclei per millimeter of fiber length in rodents 21 days following synergist ablation, achieved by excising 2/3 of the distal end of the tibialis anterior muscle (Goldberg, 1967; Bruusgaard, Johansen, Egner, Rana, & Gundersen, 2010). Decreasing the myonuclear domain by 16% from baseline to 6-10 days after ablation, effectively increasing the myonuclear density in the given muscle (Bruusgaard, Johansen, Egner, Rana, & Gundersen, 2010). Despite the lack of increased myonuclei

after traditional resistance training (Blocquiaux, et al., 2020; Psilander, et al., 2019), Bjørnsen et al. (2019) showed that humans performing blood flow restriction low load RT increased myonuclear number after 3 and 10 days by 21 ± 17 % and 30 ± 24 % respectively in type-I fibers, while type-II fibers increased 19 ± 18 % and 31 ± 27 %, respectively. The observed myonuclear addition superseded increase in fiber CSA, corresponding to a -13 ± 12% decreased myonuclei per fiber CSA in type-I post day 3, and -10 ± 13%, -20 ± 15% and -16 ± 14% in type-II fibers, on day 4, post 3 and post 10 respectively (Bjørnsen, et al., 2019). These studies at least indicate that cell population proportion changes might occur due to myonuclear addition and retention in a non-concomitant time course to hypertrophy and atrophy in skeletal muscle.

2.4.2 Immune cell infiltration following resistance exercise

Resistance exercise, particularly when inducing muscle damage, is known to elicit an immune response, characterized by the infiltration of various leukocyte populations to the site of damage. This process, while not fully elucidated, has substantial implications for skeletal muscle remodeling, repair, and growth following muscle-damaging resistance training. Several studies have shown substantial infiltration of multiple leukocyte populations after eccentric RT, that persists during muscle repair, regeneration and growth (Paulsen, et al., 2010; Rigamonti, Zordan, Sciorai, Rovere-Querini, & Brunelli, 2014; Burzyn, et al., 2013). Previous studies have observed an almost immediate increase in leukocyte counts as early as 30 minutes following eccentric RT. Peaking around 4-7 days post-exercise, demonstrating a substantial increase in CD16 (~7-fold increase) and CD68 cells/mm2 (~3.7-fold increase) compared to control muscle (Rigamonti, Zordan, Sciorai, Rovere-Querini, & Brunelli, 2014; Paulsen, et al., 2010). Other research, although less directly representative of RT-induced muscle damage, has demonstrated significant infiltration of regulatory T (Treg) cells following cytotoxic exposure in dystrophic mice. In addition, there seemed to be large inter-individual variability in the peak absolute number of CD45 (12870±5140 cells/mg of tissue) and TCRβ (198±84 cells/mg of tissue) (Burzyn, et al., 2013). However, a review of the literature has concluded that to inflict exercise-induced muscle damage, unaccustomed, isolated, maximal eccentric actions over large ranges of motion is necessary (Paulsen, Mikkelsen, Raastad, & Peake, 2012). Even with these criteria met, there was large inter-individual variability in the degree of muscle damage,

measured as a reduced force-generating capacity. Although some myofibrillar disruption might occur, accustomed traditional resistance training is unlikely to cause substantial muscle damage, if any. Therefore, following a less than 20% reduction in force-generating capacity and a complete recovery in the following 48h, leukocyte infiltration is hardly detectable or completely absent (Paulsen, Mikkelsen, Raastad, & Peake, 2012). Although, none of these studies directly measured cell population proportion changes following RT induced muscle damage, they clearly show potential short, moderate, and long term, yet transient skeletal muscle infiltration of multiple cell populations, which may confound the whole tissue (i.e. myonuclei plus interstitial cell, MYO+INT) epigenome.

3.0 Aim of the study

The transformative role of exercise in eliciting alterations in DNA methylation patterns has become increasingly clear over the past decade, suggesting that DNA methylation may be an important mechanism for how skeletal muscle adapts to exercise. However, these findings stem from studies conducted in whole muscle tissue, obscuring potential distinct methylation changes within myonuclei versus non-muscle cells (termed interstitial cells that are embedded between the muscle fibers) in human skeletal muscle (Sharples, Stewart, & Seaborne, Does skeletal muscle have an 'epi'-memory? The role of epigenetics in nutritional programming, metabolic disease, aging and exercise, 2016; Seaborne R. A., et al., 2018; Seaborne R. A., et al., 2018; Barrès, et al., 2012; Turner, Seaborne, & Sharples, 2019; Maaser, et al., 2021). Recently, exercise has been shown to induce a differential DNA methylation response between myonuclei and interstitial cells within rodent skeletal muscle tissue (Von Walden, et al., 2020; Wen, et al., 2021). However, in human muscle, the extent to which such changes in DNA methylation occur directly inside (via myonuclei) or outside (via interstitial cells) of the muscle fiber is still largely unexplored. This is important given that myonuclei contributes about half of the total nuclei in rodent muscle compared to the much larger proportion (~70-80%) of myonuclei observed within human skeletal muscle (Bengtsen, et al., 2021). Therefore, the lower relative proportion of myonuclei in rodents may explain such distinct differences in DNA methylation that may or may not occur in humans where the majority of nuclei is located within the muscle fiber itself.

Understanding the extent and specific locations of these methylation changes within human muscle tissue is crucial, not only for a comprehensive understanding of muscle biology and adaptation but also for potentially informing targeted interventions to enhance muscle function, recovery, and disease prevention. As such, our primary aim is to investigate the specific DNA methylation response to chronic resistance exercise within purified myonuclei from human skeletal muscle. To achieve this, we have employed Magnetically Activated Cell Sorting (MACS), a cost-effective method that has previously demonstrated >95% purity (confirmed by FACS) in isolating myonuclei from heterogeneous skeletal muscle samples (Bengtsen, et al., 2021). The use of MACS, combined with the myonuclei-specific marker pericentriolar material 1 (PCM1), will allow us to isolate and contrast the methylome in human skeletal muscle before and after a 7-week period of resistance training, comparing results from whole muscle tissue (MYO+INT) to those from myonuclei alone (MYO).

In addition, given that Wnt signaling has been shown to be differentially methylated in myonuclear promoters versus interstitial nuclei promoter regions following physical activity in mice (Wen, et al., 2021), our secondary aim is to determine whether similar differential methylation patterns in Wnt signaling persist in human skeletal muscle following resistance training. This aspect of the study is of particular interest, as Wnt signaling pathways are known to play a crucial role in muscle development and regeneration (Girardi & Le Grand, 2018). By investigating the epigenetic regulation of these pathways in response to exercise, we hope to contribute to the broader understanding of how exercise-induced epigenetic changes can impact muscle function and adaptation.

Finally, if the exercise stimulus is high enough, the potential resultant immune response may cause immune cell infiltration into the skeletal muscle. To address this potential confounder, we aim to incorporate the potential influence of immune cell infiltration and the resultant epigenetic changes in our study design and analysis.

Based on these aims, we propose the following hypotheses:

Hypothesis 1: The myonuclear methylome (MYO) significantly differs from the whole tissue methylome (MYO+INT) both in untrained and trained human skeletal muscle.

Hypothesis 2: The resistance training induced changes in DNA methylation significantly differ in MYO vs. MYO+INT. Specifically, we hypothesize that the Wnt signaling pathway follows a similar pattern as in mice, with a larger hypomethylation in MYO following RT.

Hypothesis 3: The infiltration of immune cells following resistance training will result in differential DNA methylation profiles in the whole muscle tissue sample (MYO+INT) compared to the myonuclei alone (MYO), and that MYO+INT differential methylation will be associated with immune response pathways.

4.0 Methods

4.1 Study participants and ethical approval

Twelve healthy males gave informed, written consent to participate in the following study, after successfully completing a pre-biopsy screening as approved by a physician. One participant was excluded due to not meeting the inclusion criteria, and one participant dropped out after familiarization due to a previous yet undisclosed knee injury that was aggravated by the RT program. A third participant dropped out after 5 weeks of RT due to work related time constraints. Therefore, 9 healthy males completed the entire intervention. Ethical approval was granted by the local ethical committee at the Norwegian School of Sport Sciences (NIH application number 238-080922), and data handling was approved by Norwegian center for research data (NSD ref.no. 376825). All methods were pre-approved and performed in accordance with the relevant ethical guidelines and regulations.

4.2 Study design

Nine previously untrained male participants (Table 1.) completed the training intervention of 3x/week of RT for 7 weeks. Adherence of participants to all lower-limb sessions (representing the muscle analyzed) was 95.8 ± 3.1% with 80% adherence to all the supervised RT sessions. The study was designed as a within participant design for condition (1. myonuclei vs. 2. all nuclei from the same participants SkM tissue biopsy) and over time (1. Post training vs. 2. Baseline). With all participants performing-the same RT protocol.

Table 1

	Gender	N	Height (cm)	Weight (Kg)	BMI	Fat (%)
Participants	Male	9	182 ± 6	78.15 ± 10.32	23.5 ± 2.9	24.2 ± 5.6

Baseline characteristics. All values are mean ± sd, unless otherwise stated.

The study is designed as a within participant tissue comparison, therefore all participants performed the same RT protocol. The RT protocol consisted of two lower-limb focused sessions (Monday and Friday) and one upper body-focused session (Wednesday). The leg session consisted of seven exercises: barbell back squat, machine leg press, leg extension, leg curl, Nordic curl, dumbbell lunges and stiff legged calf press, while the upper body session consisted of five exercises: barbell bench press, machine shoulder press, latt pulldown, standing dumbbell row and cable triceps pushdown. All exercises were performed for 8-10 repetitions and 4 sets, with a target rate of perceived exertion (RPE) of 9, with 90-120 seconds rest between sets and 2-3 min rest between exercises. For the first one-two exercises, participants performed one warmup set in addition to 10 min of steady state exercise on either stationary cycle ergometer, rowing machine or ski-ergometer. When participants could not perform all 10 repetitions for all 4 sets, or the RPE was above 9, the resistance was kept the same. But when RPE dropped below 9 the participants were urged to increase load by a small increment, and if RPE dropped below 8 the load was increased by a larger increment. This progressive loading can be seen in Figure 3, as a gradual increase in volume load for the lower limb sessions, calculated as weight * repetitions * sets * exercises normalized for baseline lean body mass per participant.

Prior to the RT intervention, all participants performed a familiarization week in order to accustomise to the training and exercises, marked as session -1 and 0 in figure 3. Session -1 was performed with minimal resistance with focus on exercise technique alone, while in session 0 the load that participants could perform 4 sets of 8-10 repetitions for each exercise on an individual basis was determined.

To account for learning effects, participants performed isometric strength measures and muscle cross sectional area measures (methods described below) were taken prior to session -1 and session 0 (Figure 3). Body composition was measured, and skeletal muscle tissue was sampled prior to upper body session in the familiarization week, ~48h after the first familiarization session. Due to work constraints, one

participant performed the body composition and SkM sampling 24h after first familiarization session. All post test and tissue samples were collected 4-5 days after the final RT session, to minimize the impact of any acute molecular responses and muscle swelling.

After all participants had finished the RT intervention, SkM samples were homogenized and split into two identical replicates. The first replicate contained the whole tissue homogenate containing all SkM derived nuclei i.e. both muscle nuclei/myonuclei (MYO) plus all other cell nuclei resident in a muscle tissue sample, referred to as the interstitial nuclei (INT). Therefore, we refer to the muscle homogenate as myonuclei + interstitial nuclei (MYO + INT). The second replicate underwent magnetically assisted cell sorting (MACS) to enrich and purify just a population of myonuclei (referred to as MYO). Following homogenization and isolation, DNA was isolated from both samples i.e. from both 1. MYO and 2. MYO + INT nuclei samples and analyzed for the individual genome wide DNA methylation. Briefly, the differentially regulated CpG sites and the corresponding genes were compared within each participant from baseline to post 7 weeks RT, to identify the effect of chronic RT on human myonuclear (MYO) methylome compared with myonuclear and interstitial methylome (MYO + INT).

4.3 Body composition and strength tests

4.3.1 DEXA

Whole-body fan beam Dual-Energy X-ray Absorptiometry (DEXA, Discovery QDR series) was performed at baseline in the morning (8-10 AM) following an overnight fast, ~48h after the familiarization session (session -1) (Figure 3.) and post training ~48h after last RT session, to assess anthropometric and body composition measures. All DEXA scans and segmentation of the individual limbs were performed by the same operator for all participants and all timepoints. Briefly, segmentation of the legs was set perpendicular to the mid-point of the femoral neck, and segmentation of the arms was set at the border of the glenohumeral jount to the highest point of the armpit. Quality of scans and segmentation was approved by experienced biotechnician.

4.3.2 CSA

m. Vastus lateralis and m. recuts femoris cross sectional area (CSA) was assessed by repeated panoramic ultrasound imaging (HD11XE, Phillips). CSA scans were

performed prior to isometric strength measures before session -1 and 0, to assess coefficient of variation between repeated scans, and 4-5 days after the last RT session. All scans were performed by the same operator, for a total of 5 scans per muscle per timepoint. Any poor scans would be retaken (defined as failed stitching of the panoramic image), and if operator was unsure of scan quality a 6th scan would be taken. Scans were taken on the non-dominant leg at 50% of the distance between the lateral epicondyle and trochanter major, where a transverse line was made across the entire quadricep muscle to guide the ultrasound probe. To maximize the reproducibility, a plastic sheet was laid on the skin and major landmarks would be marked, such as the proximal edge of the patella, scars and moles as well as the transverse line. At subsequent timepoints, the scanning position would be reidentified with the plastic sheet. In addition, the best scan from the first timepoint at baseline would act as a reference for all other timepoints, where major landmarks in the muscle and surrounding tissue were matched before acquiring the post training scans.

Measurement of CSA from the panoramic ultrasound scans was performed in ImageJ (version 2.3.0/1.53q; Java 1.8.0_322 [64-bit]). To measure the CSA, the global scales were set to match scales from the captured dicom file metadata. Next the contrast was enhanced by two percent to enable adequate visualization of the fascia and the inside border of the muscle fascia was marked using the polygon selection tool. All scans for each participant were analyzed consecutively to ensure the same structure would be referred to as the inside border of the muscle fascia. Coefficient of variation (CV) was calculated for each muscle across all timepoints by calculating the standard deviation and dividing it by the mean CSA for each participant per timepoint per muscle, and then multiplied by 100 to get the percent CV. The CV for the RF was 1.78% and the VL 1.52%. In addition, the reproducibility of the scans was assessed by calculating the CV between the mean of the first (baseline) and the mean of the second timepoint (post training) where the CV for RF was 1.31% and VL was 1.22%.

4.3.3 Isometric strength

Following the ultrasound scans for CSA measures, isometric strength tests were performed in an isometric dynamometer (HUMAC NORM^{TM}, CSMi Medical Solutions, software version 10.000.0026) at 90º, 60º and 30º of knee flexion. The participant

performed 10 min general warmup on stationary bike, before undergoing isometric test protocol. This was separated by 2 min brakes between angles and 30 sec between repetitions, the participant performed three consecutive maximal effort isometric leg extensions, and one leg curl at 90º, 60º and 30º knee angles. The machine setup was standardized between timepoints with a hip angle of ~90º, and torque measurement was gravity corrected for limb weight at 60º knee angle. Peak torque for each angle was acquired by isolating the highest torque value across all repetitions for each knee angle.

4.4 Muscle biopsies and sample preparation

Resting human vastus lateralis muscle were sampled in the morning (7-9:30 AM) in a fasted (overnight) at baseline and post training timepoints. The baseline sample was taken ~48 hours after first familiarization RT session -1 (Figure 3.), and the post sample was taken 4-5 days after last RT session. Bergstrom biopsy was performed ~10% distally from the midpoint between the trochanter major and lateral epicondyle of fibula, avoiding areas of immediate proximity to any previous incisions. Tissue samples of ~60-180 mg were dissected clear of adipose and connective tissue with sterile scalpel on a sterile petri dish, then flash frozen in liquid nitrogen before being stored at -80°C awaiting further processing. Prior to dissecting, the most intact piece of visible muscle fibers was cut square, suspended in optimal cutting temperature compound (OCT) and flash frozen in isopentane chilled to -120°C, before storing at -80°C until further processing.

4.5 Homogenization and myonuclear isolation

During the cell cycle of dividing cells, Pericentriolar material 1 (PCM1) is related to the centrosome and plays an important role in microtubule organization and centrosome proteostasis (Dammermann & Merdes, 2002). As SkM satellite cells mature into post-mitotic myocytes, at which point the nuclei are incorporated into SkM fibers, PCM1 re-localizes to the nuclear envelope where it forms an insoluble matrix. As such, PCM1 is found in the nuclear envelope of myonuclei in adult SkM tissue (Kubo & Tsukita, 2013; Srsen, Fant, Heald, Rabouille, & Merdes, 2009). Recently, a PCM1 antibody was used to specifically label myonuclei in cryosections of complex SkM tissue from humans and rodents. It is unclear if these human samples were obtained from a rested or trained

state, however, PCM1 antibody did not produce false positive labeling after overload in rodent muscle (Winje, et al., 2018). Using this PCM1 antibody, Bengtsen et al. (2021) were able to develop a method to isolate myonuclei from homogenized human and rodent SkM tissue with MACS, to yield >95% purity quantified through light microscopy. Further, they show that myonuclear purification is necessary for accurate representation of the epigenetic landscape in muscle cells to discern the role of epigenetic mechanisms in regulation of muscle differentiation and plasticity (Bengtsen, et al., 2021). Further validation of PCM1 as a specific marker of myonuclei found that in very specific cases, substantial false positive labeling could occur (Viggars, et al., 2023). False positive labeling mainly occurred in heavily overloaded, damaged and necrotic SkM tissue, observed after 200 electrically stimulated eccentric contractions in two human subjects (Viggars, et al., 2023). Under normal resistance training and rested conditions, the impact of false-positive identification of interstitial cells with PCM1 would therefore probably be minimal. Roughly nine percent of PAX7 positive nuclei were also PCM1 positive. However, for every 100 myonuclei, they identified 1-5 satellite cells (Viggars, et al., 2023). A ~9% false positive labeling here would mean an instance of 0.09-0.45 satellite cell nuclei per 100 myonuclei. Therefore, the PCM1 and PAX7 positive labels, showed PCM1 labeling around the centrosome, and would potentially be less impactful when sorting intact myonuclei through MACS (Viggars, et al., 2023). Therefore, we proceeded with the following method for isolating myonuclei from human SkM at baseline and after 7 weeks RT.

4.5.1 Homogenization and splitting

Myonuclei was isolated using a modified method from Bengtsen et al. 2021. Myonuclei were isolated from all nine baseline and post RT samples, where baseline and post samples from the same subject were always ran at the same time to minimize variability. Prior to myonuclear isolation, all buffers were prepared and stored appropriately until day of use. On the day of isolation, 1x protease inhibitor (Complete Protease Inhibitor Cocktail, Roche) was added to all buffers, and 10 U/ml (0.25 ul/ml of 40 U/ul stock) RNase inhibitor (Protector RNase Inhibitor, Roche) was added to all buffers involved with homogenization and filtering. The muscle tissue was transferred from -80˚C freezer to -20˚C cryostat, where the tissue was minced with a sterile blade into pieces of less than $1mm^3$. The minced tissue was then transferred to gentleMACS

M-tubes (Miltenyi Biotec) and stored at -80˚C. On the day of isolation, samples were transferred to ice and thawed for 2-5 min in 4 ml of lysis buffer (10 mM Tris-HCl pH 7,6 (cold adjusted), 5 mM CaCl2, 3mM MgAc, 2 mM EDTA, 0,5 mM EGTA). Samples were then homogenized using a gentleMACS Dissociator (Miltenyi Biotec) set on default homogenization program (protein_01) for a total of three cycles, and placed on ice between each cycle. Following homogenization, the lysate was diluted in 4 ml of lysis buffer with 0.4% Triton X-100, and then filtered through a 100 µm strainer and then a 40 µm strainer (Falcon, Sigma Aldrich) to remove large tissue aggregates. The filters were then rinsed with 2 ml of lysis buffer + 0.2% Triton X-100. The total lysate of ~11ml was centrifuged with a swing-out rotor at 1000g for 5 min at 4˚C, and the supernatant was carefully removed without disturbing the pellet. The pellets were resuspended in 500 µl of nuclei staining buffer (5% BSA wt/vol, 0.2% IGEPAL–CA630, 1 mM EDTA in sterile Phosphate Buffered Saline (PBS)) containing an antibody against PCM1 (1:1000, HPA023370, Sigma Aldrich). From the ~550 µl supernatant, 85 µl was allocated to homogenate tissue (MYO + INT) DNA isolation, 250 µl was allocated for homogenate tissue (MYO + INT) RNA isolation and the rest continued through to myonuclear (MYO) isolation. MYO + INT RNA fraction was added to 500 µl of trizol, vortexed and stored in -20˚C freezer for later downstream isolation of RNA. MYO + INT DNA fraction was added to 200 µl DNA lysis buffer (180 µl of ATL buffer and 20 µl of proteinase k, DNeasy Blood and Tissue Kit; Qiagen, United Kingdom) and stored in -20˚C freezer for downstream isolation of DNA.

4.5.2 Myonuclei isolation

The remaining fraction of sample in staining buffer was incubated on tumbler set to 40 rpm for 1 hour at 5˚C, then centrifuged for 1 min at 1000g with slow acceleration at 4˚C. Supernatant was carefully removed without disturbing the pellet, and the pellet was washed in 500 µl sorting buffer (1% BSA wt/vol, 2% skimmed milk powder (Sigma Aldrich) 1 mM EDTA in sterile PBS and filtered through 40 µm syringe filter (Sigma Aldrich). The pellet was broken up by pipetting up and down ~5 times, before the sample was centrifuged again for 1 min at 1000g with slow acceleration at 4˚C. The supernatant was removed, and the pellet was resuspended in 80 µl sorting buffer and 20 µl secondary Anti-rabbit IgG MicroBeads (Miltenyi Biotec), and incubated for 15 minutes at 4˚C. After incubation, the samples were centrifuged and washed once as

described above, resuspended in 1 ml of sorting buffer and incubated on tumbler set to 40 rpm for 5 min at 5˚C. After incubation, the samples were carefully applied to the center of a pre-washed (500 µl sorting buffer) M column (Miltenyi Biotec), washed 3 times with 500 µl sorting buffer and eluted with 1 ml sorting buffer after removal from the magnet. The eluates were applied to another M column, washed 3 times with 500 µl sorting buffer and eluted in 1 ml sorting buffer. The eluted samples were centrifuged for 5 min at 800g with slow acceleration at 4˚C. Following centrifugation, the supernatant was removed, except for the last ~50 µl, and resuspended in 150 µl of staining buffer and 200 µl DNA lysis buffer, before storage in -20˚C freezer prior to DNA isolation.

4.5.3 Quantification of nuclei in MYO + INT and MYO alone aliquots

Before storage, 10 µl of sample was taken from all aliquots and diluted in staining buffer, 1:6 for MYO + INT samples and 1:4 for MYO samples. Hoechst was then added at a final concentration 1:1000 to stain the DNA for quantification of nuclei numbers in samples. ~1-2 µl of diluted and stained sample was added to a hemocytometer and manually counted under a fluorescent microscope.

4.6 DNA Isolation, Bisulfite Conversion and Methylome Wide BeadChip Arrays.

All DNA samples were isolated using a commercially available DNA isolation kit (DNeasy Blood and Tissue Kit; Qiagen, United Kingdom) in accordance with manufacturers' instructions on the same day. Samples were collected from -20°C and thawed on ice. Samples were supplemented with 200 µl of AL buffer before incubation for 10 min at 56°C. Molecular grade ethanol (200 µl of >96% pure EtOH) was subsequently added to the samples followed by a brief vortex and added into spin columns placed in 2 ml collection tubes (DNeasy Mini Spin Colum, DNeasy Kit, Qiagen). Spin columns were centrifuged for 1 min at 6000 g, and the collection tube was emptied carefully to not touch the column. The spin columns were washed with 500 µl of buffer AW1 and centrifuged for 1 min at 6000 g, before discarding the flowthrough again. Buffer AW2 was then added to the spin column and centrifuged for 3 min at 20000g to dry out the membrane. Spin columns were then transferred to RNA/DNA free tubes (RNase-free Microfuge Tubes, AmbionTM, ThermoFisher

Scientific, United States). The spin columns were eluted twice by adding 25 µl elution buffer AE directly to the dried membrane and centrifuged for 1 min at 6000g before adding the flowthrough back on the membrane again and repeating the centrifugation. To elute the maximal amount of DNA without diluting the DNA concentration, the spin column elution, as described above, was repeated in a second RNA/DNA free tube. A total of 50 µl of elute per sample, divided in two tubes was analyzed for DNA quantity and quality (A260/A280 ratio 1.7±0.1) by means of ultraviolet spectroscopy (QIAxpert, ThermoFisher Scientific, United States).

There was an average of 923 ± 638 ng DNA per sample. De-identified samples were then shipped on dry-ice to Queen Mary University of London's Genomic Centre for processing and DNA methylome quantification. Three samples had lower DNA yield of between 125-250 ng. However, based on Christansen et al. (2022), 125-250 ng DNA is sufficient for input into the Infinium 850K MethylationEPIC BeadChip (Figure 3).

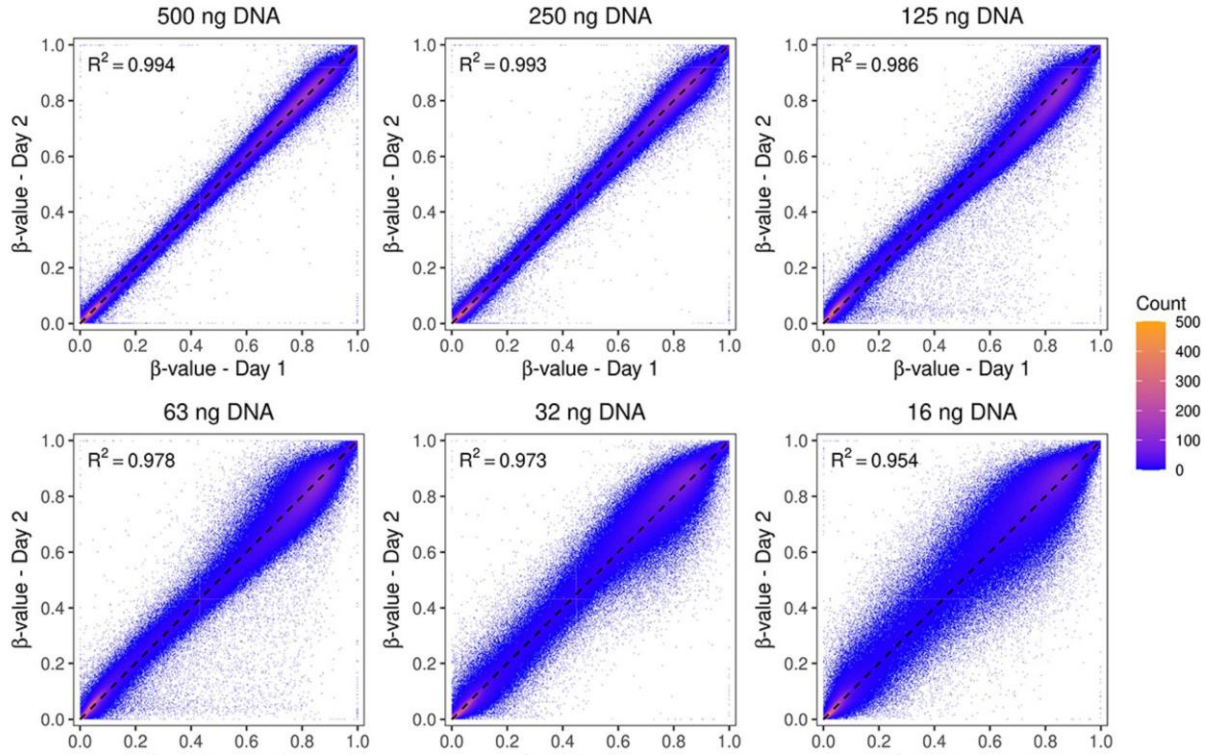

Figure 3. Christiansen et al. (2022): correlation between same samples of different DNA amounts.

The Illumina EPIC Beadchip array comprised of individual beads holding an oligo of 23 nucleotides to identify their physical location on the chip and a 50 nucleotide probe. The probe sequence is complementary to specific 50 nucleotide regions of bisulphite converted genomic DNA, with a CpG site at the 3´ end. After hybridization, the probe

incorporates a fluorescently labelled ddNTP, which allows for the quantification of proportion methylation at a particular CpG site. The proportion of DNA methylation (β-value) is calculated by $\beta = \frac{\text{methylated signal}}{\text{unmethylated signal}} + \text{methylated signal} + 100$. From this equation you are left with β-value between 0-1, where $0 = \text{completely unmethylated}$, while $1 = \text{completely methylated}$ (Pidsely, et al., 2016).

4.7 Statistical analysis

All data processing and analysis was performed in R 4.2.2 and R studio RStudio 2022.07.2 build 576. Unless otherwise stated, all values are mean and standard deviation. Unless otherwise stated, all figures were generated with the ggplot2 R package (version: 3.4.0). Change in total volume load from first session to last session was performed with a paired t-test, excluding values from participants that missed the last RT session.

4.7.1 Methylation data pre-processing

We performed the pre-processing, quality control, filtering and normalization of the DNA methylation data based on a modified version of the Bioconductor guide: “A cross-package Bioconductor workflow for analysing methylation array data” (Maksimovic, Phipson, & Oshlack, 2023). First we started by loading the red and green channel raw intensities from Illumina .idat files, using the champ.import function (ChAMP 2.26.0). All samples had an average detection P (detP) value <0.05 and were therefore kept for further processing and analysis. Next, we identified that the first three principal components explained 57.6% of the variance in the dataset. Therefore, we performed functional normalization with the preprocessFunnorm function with numbers of PCs set to three and correcting for background and dye with noob. As suggested by Maksimovic et al. (2023), functional normalization performed well with our data, and was used for all samples and comparisons. After normalization, we used the champ.filter function, that filtered the individual probe detP values <0.01 (5,278 probes), and removed all non-CpG probes (2,913 probes). From there we filtered out SNPs (42636 probes) and cross-reactive probes (946 probes) identified in Pidsley et al. (2016). There was some overlap between the SNP and cross-reactive probe lists, which is why the number of cross-reactive probes is lower than the reference list. This left us with 804,857 remaining probes for downstream analysis. Due to beta-value

based DMP analysis resulting in severe heteroscedasticity at highly methylated and unmethylated CpG sites, we then converted the beta values to M-values with the function B2M in the ENmix R package (version 1.32.0). The M-value is a logit transformation of the beta-value, and has a more statistically valid distribution for the analysis of DMPs (Du, et al., 2010).

4.7.2 Differential methylation analysis

To identify differentially methylated probes (DMPs) in the four contrasts of interest (1. MYO Baseline vs. MYO + INT Baseline; to establish baseline methylome differences between Myonuclei compared with all nuclei in a muscle tissue homogenate, 2. MYO Post vs. MYO + INT Post; to establish post training methylome differences between Myonuclei compared with all nuclei in a muscle tissue homogenate, 3. MYO + INT Post vs. MYO + INT Baseline; to establish baseline to post training methylome differences in all nuclei in a muscle tissue homogenate, and 4. MYO Post vs. MYO Baseline; to establish baseline to post training methylome differences specifically in Myonuclei), we performed paired sample t-tests using R programming language. These statistical tests were chosen because they allow for the comparison of two related/paired samples (myonuclei/ MYO and whole muscle tissue homogenate (MYO + INT) obtained from the same subjects at different time points, thereby accounting for the within-subject variability.

First, we calculated the group averages for each contrast by converting the beta values to M-values using the B2M() function from the ENmix package (version: 1.32.0), as M-values provide better statistical properties for differential methylation analysis. We then created data frames to store the t-statistic, p-value, 95% confidence interval (CI) limits, and delta M-value for each probe in the four contrasts. We looped through each probe (n = 804,857) and performed paired sample t-tests using the t.test() function from the stats package in R (version: 4.2.2), comparing the M-values of the two groups in each contrast.

To account for multiple testing, we applied the false discovery rate (FDR) correction using the Benjamini-Hochberg method, which controls the proportion of false positives among the significant results. This method was chosen because it is less conservative than other methods, such as Bonferroni correction, and provides a good balance between sensitivity and specificity. The FDR correction was applied to the within-time

comparisons (i.e. MYO Baseline vs. MYO + INT Baseline and MYO Post vs. MYO + INT Post) using the p.adjust() function from the stats package in R. We then filtered the DMPs for each contrast based on an adjusted p-value (for within-time comparisons) or raw p-value (for between-time comparisons) of =< 0.05, which is the conventional threshold for statistical significance.

Heatmaps were generated using the heatmaply R package (version: 1.4.2), using individual β-values for all CpG Island probes that were either significant between MYO + INT and MYO before or after RT. Venn diagram of β-value skew was generated by taking all before or after RT, and looking at the methylation direction in MYO vs.MYO + INT. Venn diagram was generated with the ggvenn R package (version: 0.1.9). Venn diagram of overlapping DMPs between baseline and post MYO + INT and MYO samples was generated same as described above. Kmeans klusters were computed with the kmeans function built in to the tidyverse package (version: 1.3.2.). To find the correct number of clusters we used the elbow method. Volcano plot of individual probes was generated with the individual DMPs from MYO + INT and MYO post vs. baseline ΔM-value on the x axis and un-adjusted p-value on the logarithmic y axis. App probes with a ΔM-value under -0.8 and over 0.8, or p-value under 0.0001 was annotated with the gene name from the Illumina annotation file (Infinium MethylationEPIC v1.0 B5 Manifest File).

4.7.3 Differentially methylated regions

In addition, we performed DMR analysis on the methylation changes from before to after 7 weeks of RT, using the DMRcate method. Continuing with the calculated M-values, we split our data into MYO + INT and MYO samples, and made a design matrix of baseline and post samples corresponding to columns in the M-values dataframe. Then we annotated genomic regions of each probe using the cpg.annotate function from the DMRcate R package (version 2.10.0), setting a lenient un-adjusted p-value of 0.05 cutoff. We then used the DMRcate function to identify DMRs, setting a smoothing parameter of lambda = 1000 and a scaling factor C = 2. Finally, we extracted and annotated the DMRs to the closest downstream gene with the extractRanges function, resulting in separate DMR lists for MYO + INT and MYO.

4.7.4 Over-representation analysis of functional terms and pathways

To better understand the cellular and molecular effects and interactions of the methylation changes following 7 weeks of resistance training, we performed over-representation analysis (ORA) of molecular pathways and functional terms (KEGG and MsigDB). We performed the ORA-analysis using the missMethyl function gsameth, manually supplying the KEGG and MsigDB geneset lists (Subramanian, et al., 2005). The gsameth function tests for gene-set enrichment using Wallenius concentral hypergeometric test, accounting for the un-even number of CpG probes per gene on the EPIC array (Phipson, Maksimovic, & Oshlack, 2016). KEGG gene sets were downloaded from the gage R package (Luo, Friedman, Shedden, Hankenson, & Woolf, 2009), and MsigDB gene sets were downloaded from the online database (Subramanian, et al., 2005).

The visualization of KEGG pathways was performed with the pathview R package (version 1.36.1) with the negative and positive ΔM-value change rescaled between -1 and 0, and between 0 and 1 respectively, with the rescale function in the scales package (version 1.2.1). To identify which genes in the pathway were significant for the timepoint*sample interaction, we performed linear mixed effects modeling using the lmer function in the lme4 R package (version 1.1-31), with the M-value as the response variable, and CpG, Timepoint, Sample, their interaction (Timepoint*Sample) as fixed effects. Random intercepts were included for each participant, to account for the repeated measures within individuals. We then assessed the model assumption of normality, and the normal distribution of residuals by plotting a QQ-plot and a residuals plot respectively. The emmeans R package (version 1.8.4-1) was used to calculate the estimated marginal means for each combination of timepoint and sample using the kenward-roger method, providing the average response (mean M-value across all probes in the gene) and 95% confidence interval after controlling for the other variables in the model.

We used the same ORA method to investigate the changes in cell-population specific genes. Briefly, marker genes for muscle endothelial cells, smooth muscle cells, pericytes, FAP cells, PCV endothelial cells, satellite cells, FBN1 FAP cells, NK cells, myeloid cells, B cells, and T cells were from the “Rubenstein_skeletal_muscle” gene set in MSigDB. We then performed ORA as previously describes of DMPs from MYO

+ INT and MYO in these gene sets identified from single-cell transcriptomics (Voisin, et al., 2023).

5.0 Results

5.1 Physiological adaptation to RT

To study the effects of chronic RT on the myonuclei (MYO) specific methylome compared with the whole tissue methylome (MYO + INT), nine healthy, previously strength untrained males performed high volume RT thrice weekly for a total of 7 weeks. In addition, the participants performed one week of familiarization to become accustomed to RT and testing procedures in order to account for learning effects and delayed onset muscle soreness (DOMS). After 7 weeks, we observed increased relative volume lifted across all exercises in all participants as seen in Figure 4A. Participants increased their absolute volume load after 7 weeks of RT by 5,596±2,159kg ($p<0.0005$), an increase of 49.1±23.7% from the first session. Accompanying this RT weight increase, mean isometric knee extension strength increased at 60° knee angle by 9.4±31.7N ($p>0.05$) and at 90° knee angle by 24.8±49.8N which corresponded to a relative increase of 3±12% and 11±23%, respectively ($p>0.05$) (Figure 4B). The group mean change for isometric knee extension at 30° knee flection was -8.3±33.5N which resulted in a -2±25% (Figure 4B). Due to high inter-individual variability, none of the isometric strength measurements reached statistical significance ($p>0.05$) as seen in Figure 4B. The same was the case for isometric knee flection strength, where none of the tested knee angles led to significant ($p>0.05$) change from baseline (Figure 4C). Therefore, to investigate if the participants increased their muscle mass, we performed body composition measurements with DEXA. All participants increased whole body lean mass by 6.0±2.6% equaling 3.3±1.5kg ($p<0.0005$). In addition, we wanted to look at the lean mass in the non-dominant biopsy leg where all subsequent downstream analysis was performed. The lean mass of the non-dominant leg across all participants increased by an average of 7.6±3.4% equaling 720±284g ($p<0.0005$) (Figure 4D). To further confirm that the participants increased their muscle mass in the VL, from where we obtained the biopsy, we performed panoramic ultrasound scans of the VL approximately at the mid-belly. Again, all participants increased their VL CSA

significantly from baseline, by 18.2±5.7% equivalent to 4.3±1.3 cm^2 ($p<0.00005$) (Figure 4E). Additionally, all participants increased their RF CSA significantly from baseline by 15.6±9.1% equalling 1.1±0.7cm^2 ($p<0.005$) (Figure 4E). It's impressive to se the VL and RF CSA change from baseline (Figure 5F) to post 7 weeks RT (Figure 4G).

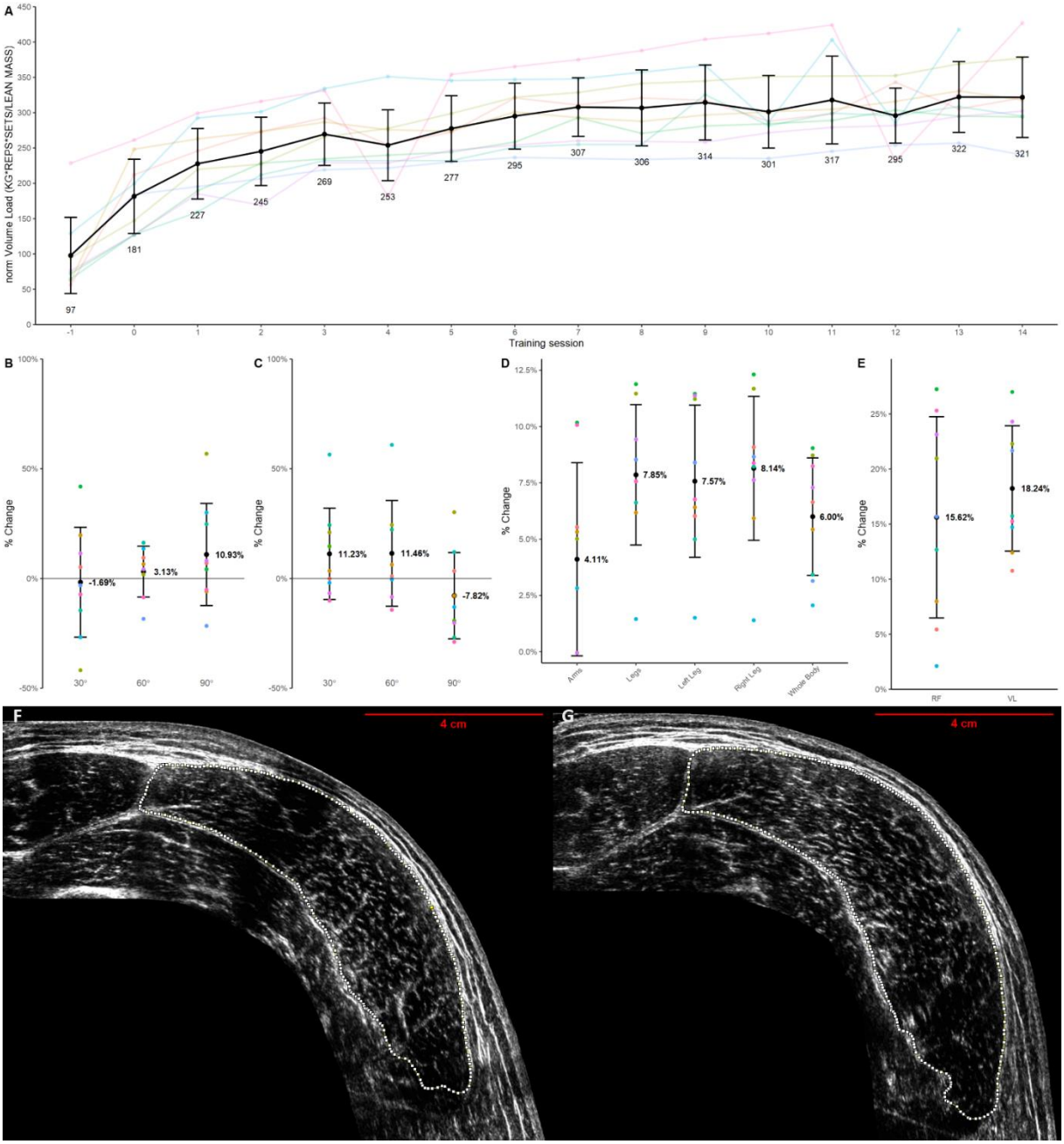

Figure 4. Black dots and error bars are group mean ± one standard deviation from the mean. Colored lines and points are individual participant data. A: Line plot of individual (colored lines) and group mean ± sd (black line) volume load per training session, normalized to baseline lean body mass, for the lower-limb sessions. Session -1 and 0 are familiarization sessions, while session 1-14 are the full lower limb RT sessions over the 7 weeks intervention period. B-C: Isometric strength change from baseline for knee extension and flexion at 30°, 60° and 90° knee angle, respectively. D: Lean mass percent change from baseline via DEXA. E: Rectus femoris (RF) and Vastus lateralis (VL) cross sectional area percent change from baseline. F-G. Panoramic ultrasound of m. Vastus

Lateralis mid belly at baseline and post 7 weeks RT, respectively, with inside border of fascia marked for CSA measurement. Images are taken from participant with the VL CSA change closest to the group mean.

5.2 Cell population specific DNA methylome in untrained and trained human skeletal muscle, myonuclei (MYO) vs. myonuclei + interstitial cells (MYO+INT)

5.2.1 DNA methylome of MYO vs. MYO+INT in untrained human skeletal muscle

To compare the epigenetic landscape specifically in myonuclei (termed MYO), we compared the DNA methylome profile of PCM1 labelled myonuclei and compared this with the methylome profile from all nuclei in a muscle tissue homogenate (termed myonuclei plus interstitial nuclei or MYO+INT) from the same biopsy/participant at rest (baseline). Therefore, we used the MYO+INT condition as the calibrator/reference as methylome data from all nuclei within the tissue homogenate has been characterized before (Gorski, et al., 2022; Maaser, et al., 2021; McGee & Hargreaves, 2019; Seaborne R. A., et al., 2018; Sexton, et al., 2023). Indeed, we identified 223,352 differentially methylated positions (DMPs) with an FDR of $p<0.05$ in MYO compared with MYO+INT. Of these, 15,506 DMPs were located in CpG islands (Figure 5A.), 9794 DMP's were located in promoters, relating to 2,123 DMPs in promoter associated CpG islands. Furthermore, 56.2% of probes (125,610) had negatively skewed β -values and 43.8% of probes (97,742) had positively skewed β-values in MYO vs. MYO+INT (Figure 5A). Therefore, to investigate further the difference in β-value at baseline, we calculated the change in β-value in DMPs at baseline in MYO compared with MYO+INT. Of these, 1,375 probes in MYO had more than 0.3 β -value difference compared to MYO+INT (Figure. 5B).

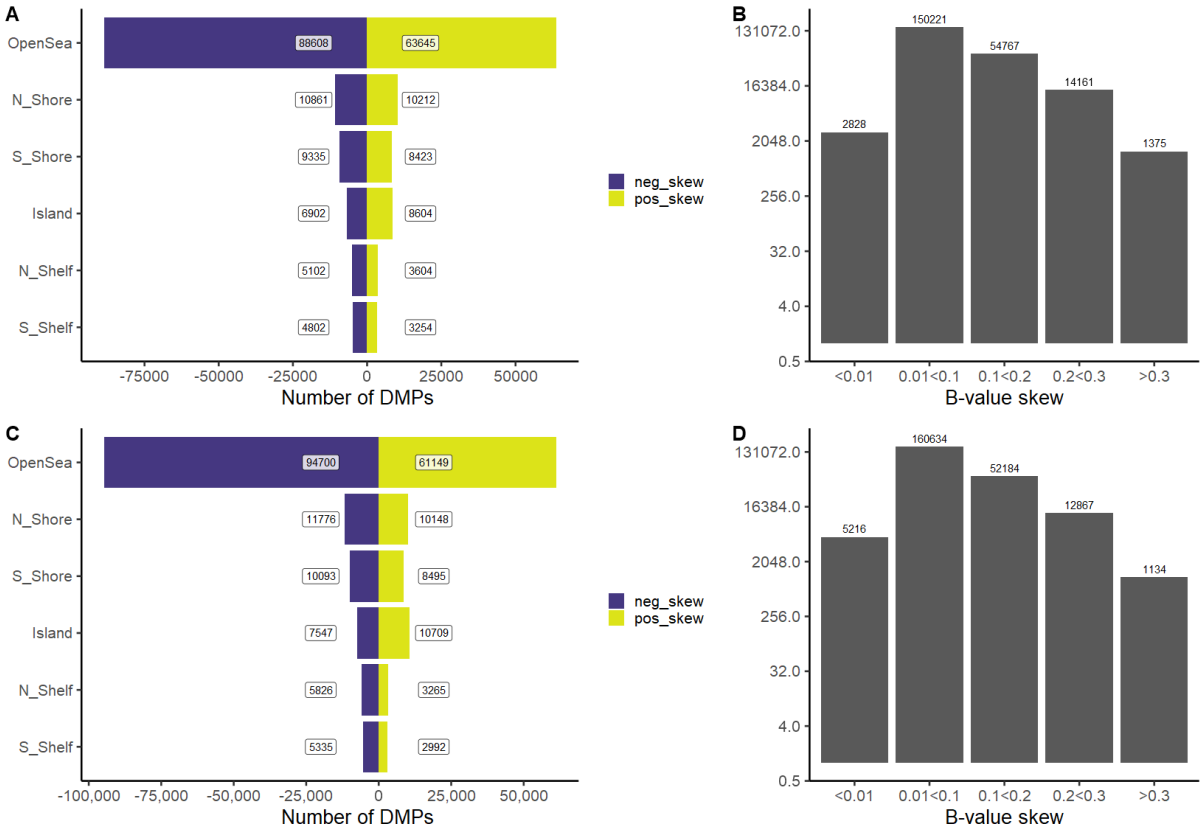

Figure 5 Differentially methylated probes in Myonuclei (MYO) vs. myonuclei + interstitial cells (MYO+INT) in previously untrained individuals and after 7 weeks of RT. A: Number of DMPs at baseline in different gene regulatory features, with direction of difference in MYO vs. MYO+INT. B: Number of DMPs at baseline by ΔB-value in MYO vs. MYO+INT. C: Number of DMPs after 7 weeks of RT in different gene regulatory features, with direction of difference in MYO vs. MYO+INT. D: Number of DMPs after 7 weeks of RT by ΔB-value in MYO vs. MYO+INT.

5.2.2 DNA methylome of MYO vs. MYO+INT in trained human skeletal muscle

To begin to identify differential methylome profiles after resistance training (RT) induced hypertrophy, specifically in myonuclei (MYO) compared with all nuclei from a muscle tissue homogenate (MYO+INT) we identified 232,035 DMPs (FDR p<0.05) in MYO compared with MYO+INT after 7 weeks of RT. Of these, 18,256 DMPs were located in CpG islands (Figure 5C), 11,506 DMP's were located in promoters, relating to 3,277 DMPs located within promoter associated CpG islands. Furthermore, 58.3% of probes (135,277) had negatively skewed β -values and 41.7% of probes (96,758) had positively skewed β-values in MYO vs. MYO+INT (Figure 5C). Again, we compared the β-value of all DMPs after 7 weeks of RT and found 1,134 probes with a Δ β-value >0.3 (Figure 5D).

5.2.3 DNA methylome of MYO vs. MYO+INT in untrained vs. trained muscle

Next, we wanted to identify the directionality of ΔM-value across the DMPs at both the baseline and post training comparisons between MYO vs. MYO+INT. We identified 107,227 DMPs that were negatively skewed before and after RT, whilst only 18,378 were negatively skewed before RT and 28,035 were negatively skewed after RT (Figure 6A). Conversely, 71,410 DMPs were positively skewed before and after RT, whilst only 26,317 were positively skewed before RT and 25,343 were positively skewed after RT (Figure 6A). In total, 64.5% of DMPs between cell populations are skewed in the same direction before and after RT. That leaves ~35% of DMPs that are only skewed at one timepoint, which would have a larger effect when looking at DMPs from before to after 7 weeks of RT.

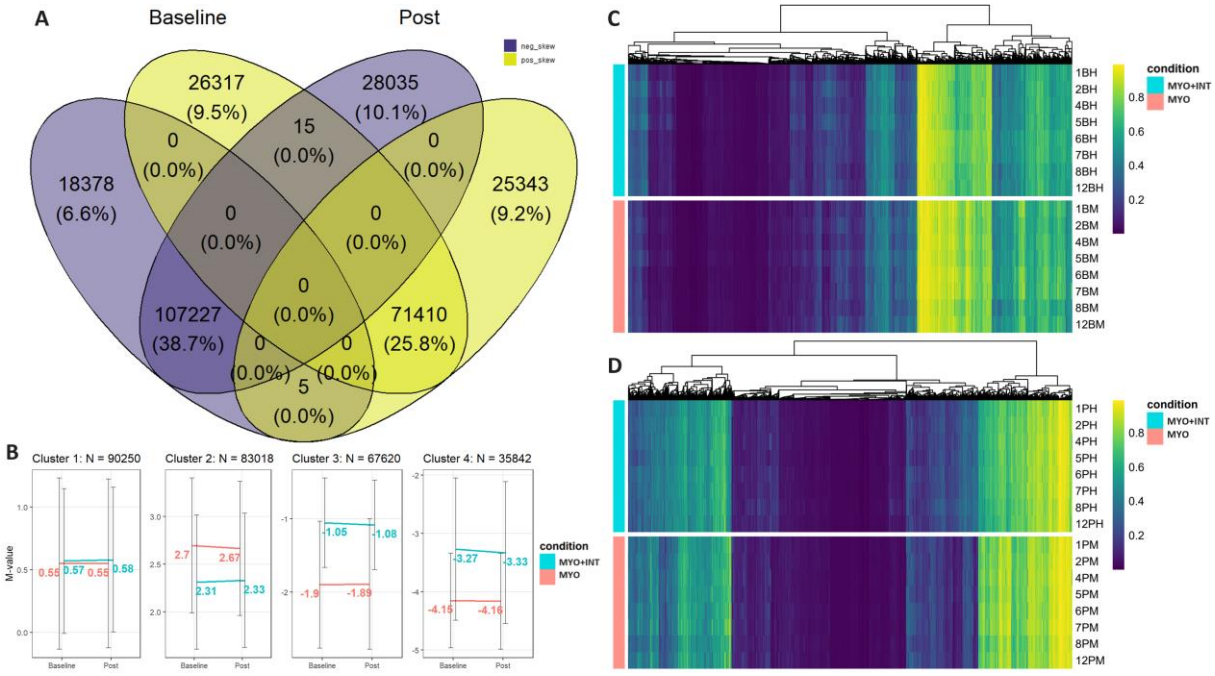

Figure 6 Characterization and comparison of myonuclei (MYO) samples compared with all nuclei derived from a muscle tissue homogenate (MYO+INT) before and after resistance training (RT). A. Venn diagram of direction of difference in MYO vs. MYO+INT. B. Kmeans clustering of all DMPs before and after RT, mean ± sd M-value for each cluster. C. Heatmap of beta values from DMPs within CpG islands in untrained muscle. D. Heatmap of beta values from DMPs within islands in trained muscle (after 7 weeks RT).

In addition, we identified the DMPs that were differentially methylated at baseline or at post between MYO and MYO+INT (Figure 6A). If the difference between MYO and MYO+INT is opposite at baseline and at post, it might lead to high likelihood for those DMPs are determined as significant when looking at the time effect within MYO+INT or MYO. Thus, we identified the 15 CpGs (cg00049674; cg00408117; cg01558037;

cg01808641; cg02165526; cg04345102; cg06431604; cg09117405; cg09638248; cg12243862; cg15966124; cg17336432; cg17993313; cg19062656; cg20368841) that were negatively skewed at baseline and positively skewed at post. Of these, 9/15 were significant in the MYO+INT, whereas only 6/15 were significant in MYO following RT. Four of the identified CpGs were significant in both MYO and MYO+INT following RT (cg12243862; cg15966124; cg17336432; cg20368841), all of which had a negative ΔM-value in the MYO and positive ΔM-value in the MYO+INT. We also identified the 5 CpGs (cg09355820; cg10429575; cg10881514; cg11202814; cg26891661) that were positively skewed at baseline and negatively skewed at post. All of which were significant in the MYO+INT while only one (cg10429575) was significant in the MYO. Interestingly, this one shared CpG had a negative ΔM-value (un.adj. p = 0.044, 95% CI: -0.375, -0.006, ΔM = -0.19) in the MYO+INT cell population following RT and positive ΔM-value (un.adj. p = 0.039, 95% CI: 0.01, 0.32, ΔM = -0.16) in MYO.

Looking at the general pattern of difference in M-values in MYO vs. MYO+INT cell populations before and after RT, we performed k-means clustering to identify the number of individual clusters. We identified the inflection point at four clusters with the elbow method, where the residual sum of squares did not substantially reduce with the addition of more clusters (Eremenko, 2018, pp. 135-144). After clustering we were left with four subsets of DMPs, of which one had seemingly no difference in average M-value per probe in MYO vs. MYO+INT (Figure 6B-1, N = 90,250). In the other three clusters, cluster two presented a subset where MYO had a higher M-value (Figure 6B-2, N = 83,018), while the remaining two clusters had a lower M-value in MYO vs. MYO+INT (Figure 6B-3, N = 67,620 & 6B-4, N = 35,842). Looking further at the subset of DMPs located within CpG islands, clustering by unsupervised hierarchical clustering shows ~3-4 main subgroups both before and after RT (Figure 6C & 6D dendrogram). Consistently across timepoints, we can see that the MYO cell population has more

hypo- and hypermethylated probes, while the MYO+INT cell populations seem to have more mid-range B-values (Figure 6C & 6D heatmap).

5. Genome-wide differential methylation after resistance training in myonuclei compared with myonuclei + interstitial cells after resistance training

Next, to investigate the effect of 7 weeks of RT on the methylome in MYO and in MYO+INT conditions, we performed DMP analysis within the same condition i.e., within MYO or within MYO+INT conditions between time (post training vs. baseline). There was no significant post training DMPs in either MYO or MYO+INT using a false discovery rate. However, differential methylation of genes within relevant resistance exercise responsive pathways have been discovered using unadjusted p-values in human studies with typically low sample sizes due to the nature of the intervention and invasiveness of human biopsies (Seaborne R. A., et al., 2018; Turner, Seaborne, & Sharples, 2019; Sexton, et al., 2023). Furthermore, discovery of important differentially methylated genes using unadjusted p-values after resistance training in human muscle, such as UBR5 (Seaborne R. A., et al., 2018), have led to the identification of gene targets that have subsequently been validated as important regulators of muscle mass (Hughes, et al., 2021; Seaborne, et al., 2019). Therefore for discovery purposes, we performed paired samples t-test with an un-adjusted $p = < 0.05$, which has previously identified differentially methylated differentially expressed genes (Gorski, et al., 2022; Maaser, et al., 2021; Seaborne R. A., et al., 2018), which identified 27,599 and 20,543 DMPs post training compared with baseline in MYO and MYO+INT, respectively. Post resistance training in both MYO and MYO+INT conditions identified that there was a larger majority of DMPs containing hypomethylated compared with hypermethylated profile (Figure 7A), as previously described in DNA methylome analysis in all nuclei derived from muscle homogenate after both acute and chronic resistance exercise in humans (Seaborne et al., 2018, Turner et al., 2019, Sexton et al., 2023). The MYO specific methylome demonstrated a greater proportion of DMPs that were hypomethylated compared to MYO+INT (MYO = 61.1% vs. MYO+INT = 51.3%, Figure 7A) corresponding to 7,056 more DMPs that were hypomethylated in MYO only compared with MYO+INT. Of all DMPs, only 1.9% / 901 DMPs were significantly altered in both the myonuclei and the MYO+INT condition after training

(Figure 7B), suggesting that 98.1% of methylation changes in the myonuclei were at different sites compared to the methylation changes taking place in the bulk nuclei in a muscle tissue homogenate. As DNA methylation changes are most likely to alter gene expression if located in CpG rich islands within regulatory regions such as promoters (Egan & Sharples, 2023), we also investigated hypo and hypermethylation of DMPs located in the different genomic regulatory features. Firstly, the largest fraction of DMPs in both MYO and MYO+INT after RT were located in the “Open Sea” regions, where we observed a significantly larger proportion of hypomethylation in the myonuclear DMPs (Figure 7C & 7D 10,357 DMPs in MYO vs. 5,588 DMPs in MYO+INT). There was also a different proportion of hypo- to hypermethylation occurring in CpG islands between myonuclei vs. MYO+INT. Interestingly, whilst across all DMPs in N_shelf, N_shore, open-sea, S-shelf and S_shore there was a greater proportion of DMPs hypomethylated in the MYO (Figure 7C) vs. MYO+INT cell population (Figure 7D), specifically in CpG islands the opposite trend occurred (Figure 7C), where in the myonuclei the majority (59%) of DMPs were hypermethylated compared with hypomethylated (41%), and in the MYO+INT cell population (Figure 7D) the majority (56.9%) were hypomethylated compared with hypomethylated (43.1%). Looking further at DMPs that were located CpG Islands within promoter regions, the effect of increasing proportion of hypermethylation in MYO conditions was further exaggerated where 70.7% of DMPs were hypermethylated and 29.3% hypomethylated (Figure 7E).

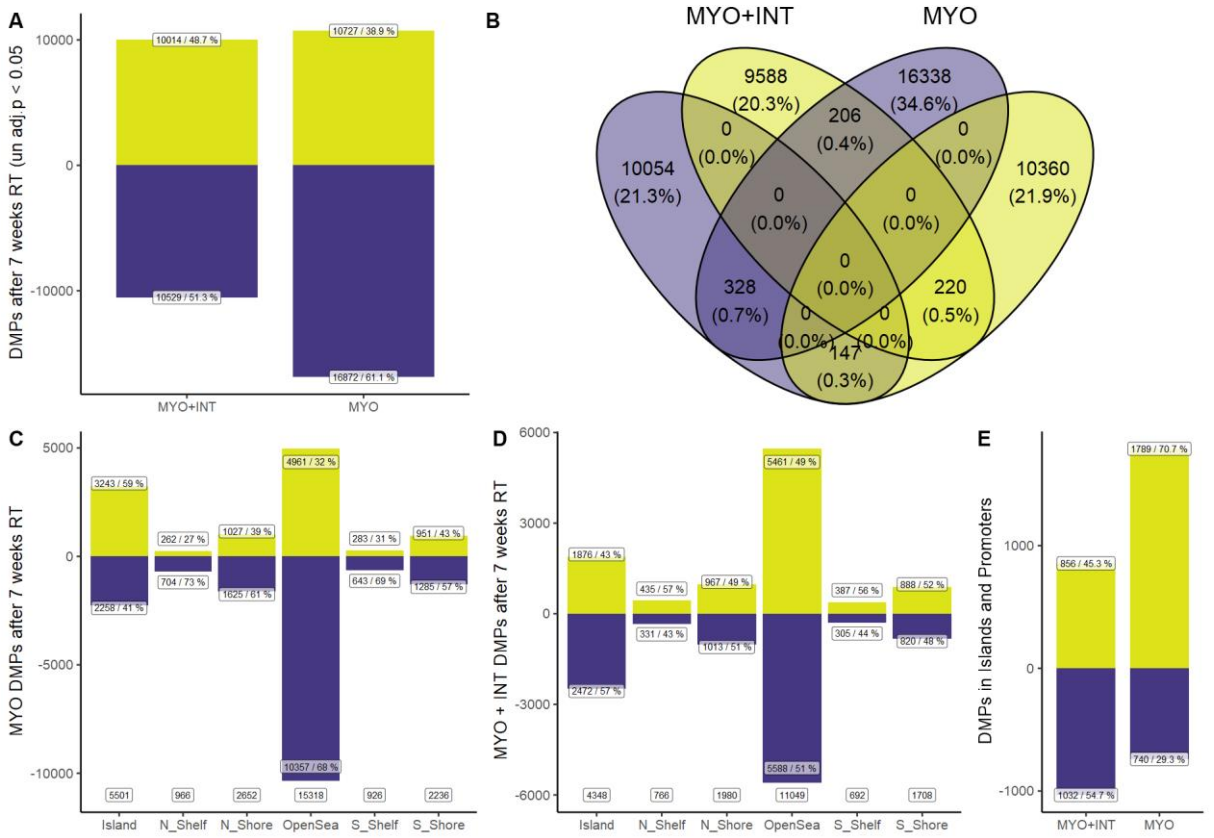

Figure 7. Differentially methylated probes following 7 weeks of RT. A. All DMPs in myonuclei + interstitial cells (MYO+INT) and myonuclei (MYO) following 7 weeks of RT. B. Venn diagram of hypo- and hypermethylated probes following RT in MYO+INT and MYO. C. All MYO DMPs following RT grouped into genomic features relative to CpG Islands. E. All MYO+INT DMPs following RT grouped into genomic features relative to CpG Islands. E. Island and promoter associated DMPs following RT.

5.3.1 Whole muscle tissue (MYO+INT) DMPs following 7 weeks of RT

After identifying ~20 000 DMPs in the MYO+INT sample following RT, we wanted to look at the most significant individual probes and the genes they are annotated to (Figure 8). In addition, we wanted to look at the difference and similarity in methylation in the same probes in the MYO sample. We identified 18 DMPs with an unadjusted p-value of =< 0.0001, 9 DMPs with a ΔM < -0.8 and 13 DMPs with a ΔM higher than 0.8 in the MYO+INT sample (supplementary file: “MYO+INT_DMPs_after_RT_volcano-plot”). Among these probes, we observed a significant difference in methylation MYO vs. MYO+INT cell populations, of which several probes displayed differential methylation patterns. Interestingly, none of the most DMPs in MYO+INT were significantly differentially methylated in MYO. The same was the case with the most differentially methylated probes in MYO+INT that were hypermethylated after RT, were not significant DMPs in MYO after RT.

Of the most differentially methylated probes in MYO+INT, 22/40 DMPs had a tendency towards hypomethylated in the MYO sample compared to hypermethylated in MYO+INT. 8 DMPs were hypomethylated in MYO+INT and hypermethylated in MYO, such as CCND1 (cg05164185, MYO+INT: p = 0.002, ΔM = -1.6, 95% CI [-2.8,-0.3], MYO: ΔM = 0.5, 95% CI [-0.7,1.8]), GPR125 (cg05898174, MYO+INT: p = 0.00009, ΔM = -0.2, 95% CI [-0.3,-0.15], MYO: ΔM = 0.07, 95% CI [-0.2,0.4]) and CXCL2 (cg23244559, MYO+INT: p = 0.049, ΔM = -1.0, 95% CI [-2.0,-0.001], MYO: ΔM = 0.05, 95% CI [-1.1,1.2]). Conversely, 9 DMPs in MYO+INT after RT were hypermethylated in MYO+INT with a tendency towards hypomethylated in MYO, such as BRAF (cg0556893, MYO+INT: p = 0.002, ΔM = 1.1, 95% CI [0.2,2.1], MYO: ΔM = -0.01, 95% CI [-0.4,0.4]), DOK6 (cg26305468, MYO+INT: p = 0.00001, ΔM = 0.2, 95% CI [0.2,0.3], MYO: ΔM = -0.03, 95% CI [-0.3,0.2]) and HPCAL1 (cg19529823, MYO+INT: p = 0.037, ΔM = 1.5, 95% CI [0.1,2.9], MYO: ΔM = -0.04, 95% CI [-0.8,-0.01]).

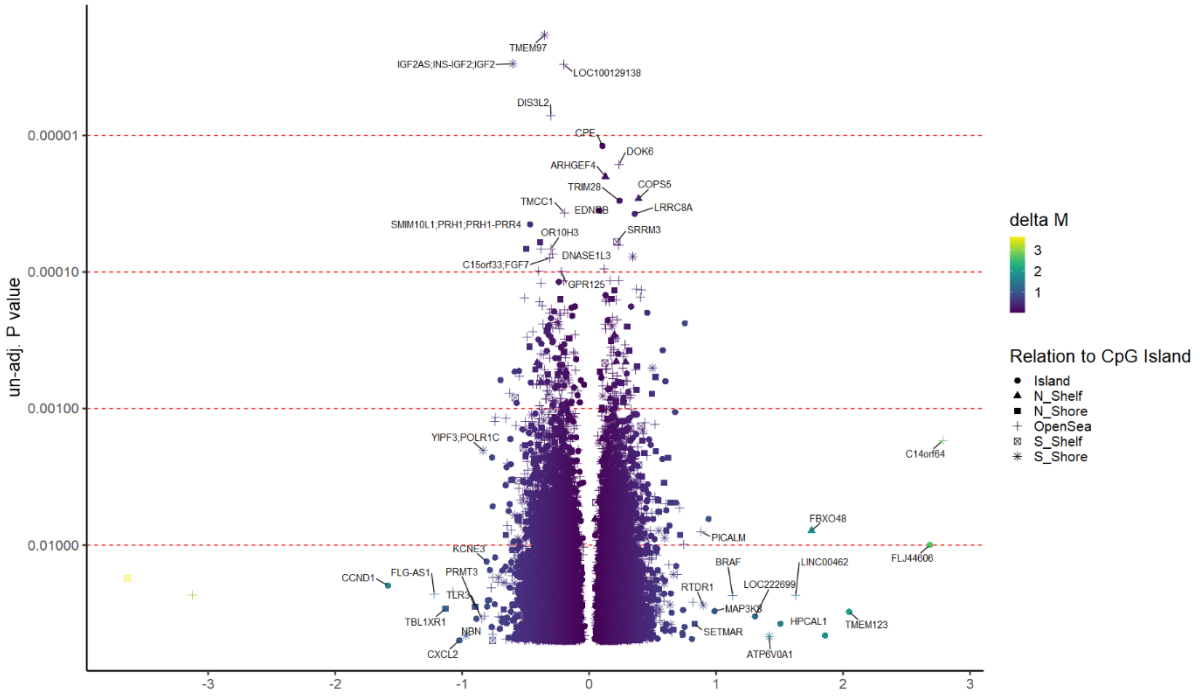

Figure 8. Volcano plot of ΔM of all significant probes in MYO+INT following RT. Most differentially methylated probes from the MYO+INT cell population are labeled with gene symbol name, identified by one of the three criteria: p-value of =< 0.0001, ΔM < -0.8 or ΔM > 0.8.

5.3.2 Isolated myonuclei (MYO) DMPs following 7 weeks of RT

Using the same criteria as for the identification of the most differentially methylated CpG probes in MYO+INT, we identified 41 CpGs with a p< 0.0001 or a M-value change

over 0.8. Interestingly, 20/41 DMPs were hypomethylated following RT (Figure 9), none of which were significant DMPs in the MYO+INT cell population. Although none of these probes were DMPs in the MYO+INT cell population, identifying which of these were hypomethylated in MYO with a tendency towards hypermethylation in MYO+INT could potentially identify myonuclei specific DMGs. In MYO, 10/41 ("IGF2", "SMAD9", "JOSD2", "FUBP1", "BANP", "STRADA", "CADM4", "MAD1L1", "HIST1H2BJ", "TNRC18") most differentially methylated probes were hypomethylated in MYO following RT, with a tendency toward hypermethylation in MYO+INT.

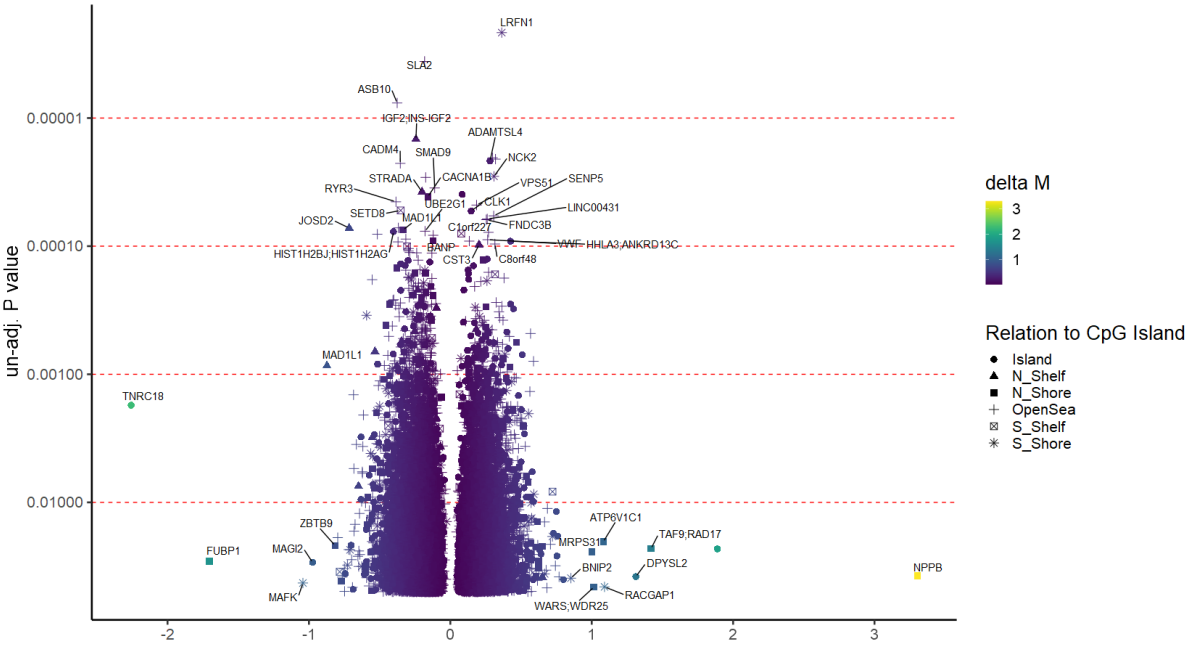

Figure 9. Volcano plot of ΔM of all significant probes in myonuclei (MYO) following RT. DMPs with a p< 0.0001 or a M-value change over 0.8 are labeled with their "symbol" gene name.

5.4 Over representation of pathways in Kyoto Encyclopedia of Genes and Genomes (KEGG) after resistance training in myonuclei compared with myonuclei + interstitial cells

Focusing on gene pathways rather than individual probes and genes provides a broader understanding of the biological implications of differential DNA methylation, and as such is a key target of the present study (Kanehisa & Goto, 2000). Using ORA-analysis, we investigate the over-representation of MYO vs. MYO+INT DMPs following RT in the Kyoto Encyclopedia of Genes and Genomes (KEGG), linking genomic

information with higher order functional information (Kanehisa & Goto, 2000). To ascertain the direction and magnitude of DNA methylation change in the pathway following RT, we calculated the average ΔM-value of all the probes in all the genes within each of the significantly over-represented pathways. Interestingly, of the 39 significant pathways in MYO+INT (un-adj. $p < 0.05$) and 52 significant pathways in MYO (un-adj. $p < 0.05$), only 14 pathways were significantly over-represented in both cell populations following RT. Six (Lysine degradation; Cell cycle; Oxytocin signaling pathway; Endocrine and other factor-regulated calcium reabsorption; Carbohydrate digestion and absorption; Transcriptional misregulation in cancer) of which observed opposite mean ΔM-value between MYO+INT and MYO. When looking at the 20 most significant pathways in MYO+INT, we observed notable differences in mean ΔM-value between MYO+INT and MYO cell populations (Figure 10). Of particular interest are the pathways that exhibit contrasting mean ΔM-values between MYO+INT and MYO, indicating cell-population specific response to RT. For instance, the Mannose type O-glycan biosynthesis pathway had a tendency towards hypomethylated in MYO (mean ΔM-value = -0.005, $p > 0.05$) compared with hypermethylated in the MYO+INT cell populations (mean ΔM = 0.008, $p < 0.05$) after RT. Similarly, the NF- κβ signaling pathway had a tendency towards hypomethylation in MYO (mean ΔM = -0.006, $p > 0.05$) compared with hypermethylation in MYO+INT (mean ΔM = 0.004, $p < 0.05$) following RT. Furthermore, the key regulator of NF-κβ activity, TNF-α was exclusively hypermethylated in a single promoter associated CpG probe in MYO (cg21467614: ΔM = 0.13, $p = 0.03$) following RT. In addition, the Endocrine and other factor-regulated calcium absorbance pathway exhibit high degree of hypomethylation in the MYO cell population (mean ΔM = -0.009, $p < 0.05$) compared with a slight hypermethylation in MYO+INT (mean ΔM = -0.002, $p < 0.05$) in response to RT (Figure 10).

The majority of the top 20 most significantly over-represented pathways in the MYO+INT sample exhibit a hypomethylated response to RT in both MYO+INT and MYO. However, 12/20 demonstrate a larger mean ΔM-value in MYO compared to the MYO+INT sample (Figure 10). Of note, are the pathways that exhibit a relatively small mean ΔM in the MYO+INT cell population, while the MYO sample is considerably more hypomethylated (ECM-receptor interaction, MYO $p > 0.05$; hsa01100 Metabolic pathways, MYO $p < 0.05$; Pancreatic secretion MYO $p > 0.05$), highlighting their potential role in the MYO cell population relative to the MYO+INT cell population.

Several other pathways such as Dopaminergic synapse, Necroptosis, Long-term potentiation and Cell cycle exhibit relatively small methylation changes and changes between MYO+INT and MYO, indicating that individual genes in the pathways exhibit highly differential methylation in both MYO and MYO+INT cell populations but the pathway demonstrates neither a predominantly hypo- nor hypermethylation. Albeit with a relatively small mean ΔM-value difference between samples, Cell cycle and Long-term potentiation were the only two pathways of top 20 that were more hypomethylated in the MYO+INT compared to MYO sample. Overall, as described above, suggesting that differentially methylated pathways are mainly hypomethylated in MYO compared with MYO+INT cell populations.

Next we wanted to take a targeted look at typical resistance exercise related pathways, specifically the energy and growth related mTOR, PI3K/Akt, AMPK and Insulin pathways. Interestingly, the primary mTOR KEGG pathway was not significantly over-represented in either sample following RT. However, the mTOR related PI3K/Akt pathway was exclusively significantly over-represented in the MYO-INT samples (MYO+INT $p = 0.004$, MYO $p = 0.18$). When taking a deeper look, the ORA revealed 202/347 differentially methylated genes (DMGs) in MYO+INT and 211 DMGs in MYO samples within the PI3K/Akt pathway. The growth/metabolic insulin pathway approached significant over-representation in the MYO sample (MYO $p = 0.07$, MYO+INT $p = 0.26$). Although the pathway did not reach a level of overall significant overrepresentation, a clear trend of hypomethylation was seen in the MYO sample (mean ΔM-value = -0.008). In contrast, MYO+INT samples leaned towards hypermethylation (mean ΔM-value = 0.002). ORA analysis discovered 75 of 137 DMGs in the MYO+INT samples within this pathway, while a slightly higher count of 90 DMGs was observed in MYO. Interestingly, the AMPK pathway involved in cellular energy homeostasis was exclusively over-represented with a hypomethylated trend in MYO

(MYO+INT p = 0.11, MYO mean ΔM = -0.007, p = 0.019). ORA of the AMPK pathway identified 71 and 84 DMGs in MYO+INT and MYO respectively.

Figure 10. Top 20 significant signaling and metabolic KEGG pathways in MYO+INT cell population, and the mean ΔM-value change following RT in MYO+INT and MYO samples. X-axis depicts the mean ΔM across all DMPs in all the genes associated to the individual KEGG pathways, indicating the overall direction and magnitude of DNA methylation change following RT.

Interestingly, the Leukocyte transendothelial migration KEGG-term was only significantly over-represented in the MYO+INT sample (p = 0.01). In Figure 10. the mean ΔM change in MYO seems to be hypomethylated compared with MYO+INT, however, Leukocyte transendothelial migration KEGG term was not significantly over-represented in myonuclei (p = 0.4) following RT. Potentially indicating an increased intramuscular leukocyte population following chronic RT, which might confound the MYO+INT epigenome compared with MYO alone.

5.5 Wnt signaling following RT in isolated MYO vs. MYO+INT

As a previously described differentially methylated pathway in mouse skeletal muscle following a resistance training model (Wen, et al., 2021), we wanted to take a more detailed look at the methylome of the Wnt signaling pathway related genes in our human samples. Using the same ORA-analysis, we found that Wnt-signaling was overrepresented in the MYO sample (p = 0.012), but not in the MYO+INT sample (p =

0.09) (Figure 11 A-B). When looking at the mean ΔM-value across all probes in all genes in the pathway, we found that Wnt was hypomethylated in MYO (mean ΔM-value change = -0.002) and hypermethylated in MYO+INT (mean ΔM-value change = 0.0004). To investigate which of the genes in the pathway that were significant for the time and sample interaction (timepoint*sample), we performed linear mixed effects modeling on the gene specific CpG-probes and their M-value, controlling for individual variability. This gave us a list of nine genes that had a significant time and sample interaction (Figure 11 C-K). Two of these genes, FRAT2 (Figure 11C) and WNT1 (Figure 11E) were the only genes that were hypomethylated in MYO+INT relative to MYO. The remaining seven genes, DVL3, AXIN1, CCDC88C, CSNK2B, LGR6, CHD8, CTBP1 were all hypomethylated in MYO relative to MYO+INT. The estimated marginal mean M-value for these nine genes in both samples and timepoints can be found in supplementary file: Wnt_emmeans.csv.

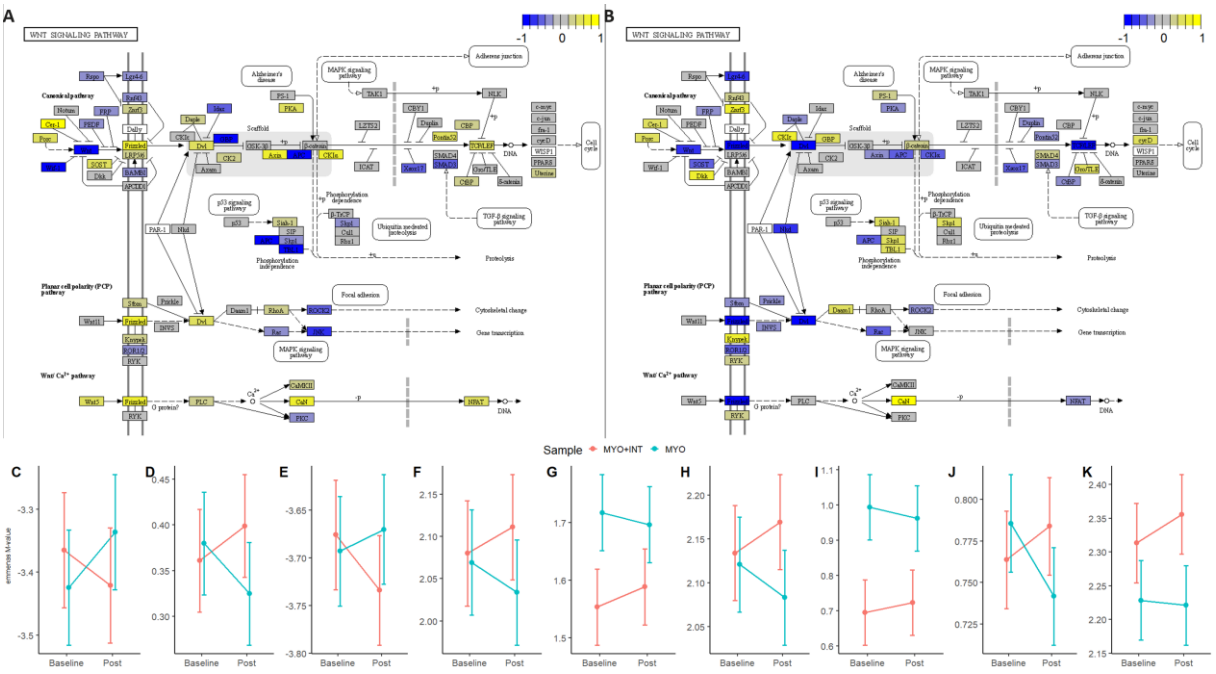

Figure 5. Differential methylation of genes in the Wnt signaling pathway (hsa04310). A-B: Interaction of genes and genomes in the Wnt pathway, colored by the scaled value of the mean ΔM-value across all CpGs in the given gene. Blue = hypomethylated, Yellow = hypermethylated *(Kanehisa & Goto, 2000; Kanehisa M. , 2019; Kanehisa, Furumichi, Sato, Kawashima, & Ishiguro-Watanabe, 2023)*. A. ΔM-value across all CpGs in the given gene in MYO+INT sample. B. ΔM-value across all CpGs in the given gene in MYO sample. C-K: All genes in Wnt pathway that were significant for time and sample interaction (timepoint*sample) from linear mixed effect model. Y axis is the estimated marginal mean M-value average across all CpGs in the given gene and 95% confidence interval. C = FRAT2, D = DVL3, E = WNT1, F = AXIN1, G = CCDC88C, H = CSNK2B, I = LGR6, J = CHD8, K = CTBP1.

The upstream inhibitor of glycogen synthase kinase 3β (GSK3β), dishevelled segment polarity protein 3 (DVL3) was identified as one of the most DMGs between MYO+INT

and MYO within the canonical Wnt – β-catenin canonical pathway following RT. DVL3 was hypomethylated in myonuclei and hypermethylated in MYO+INT ($p = 0.03$). FRAT2 which binds to DVL3 to further inhibit the downstream binding of GSK3β to β-catenin (Stoothoff, Cho, McDonald, & Johnson, 2004), was hypermethylated in myonuclei relative to MYO+INT ($p = 0.04$). In addition, AXIN1 from the axin-APC complex was identified as a DMGs with hypomethylation in myonuclei relative to MYO+INT ($p = 0.03$). CCDC88C/Daple ($p = 0.008$) and CSNK2B/CK2 ($p = 0.04$), also related to the canonical Wnt-pathway was identified as a DMG, with hypomethylation in myonuclei relative to MYO+INT. Downstream of β-catenin, CHD8/Duplin was identified as a hypomethylated gene in myonuclei relative to MYO+INT ($p = 0.024$). CHD8 has an inhibitory effect on the downstream signaling of β-catenin to TCF/LEF related to cell cycle and growth regulation. In addition, CTBP1/CtBP which directly inhibits TCF/LEF was slightly hypomethylated in myonuclei relative to MYO+INT ($p = 0.045$).

5.6 Cell population specific gene sets

Finally, we wanted to investigate the over-representation of cell specific marker genes in MYO vs. MYO+INT cell populations. Cell specific marker genes identified via. single-cell RNAseq of mononucleated cells from human vastus lateralis, which identified 11 mononuclear cell types, were downloaded from the “Rubenstein_skeletal_muscle” datasets in MsigDB (Rubenstein, et al., 2020; Subramanian, et al., 2005). As previously described, we performed ORA-analysis of MYO and MYO+INT DMPs in the cell population specific marker genes following 7 weeks of RT. The only significantly over-represented marker genes in any sample were Fibroadipogenic Progenitor cells (FAPs) and Endothelial cells, where both cell population were only significantly over-represented in MYO+INT (Figure 12). Two sub-populations of FAP-cells were significantly over-represented in MYO+INT, the FBN1+ FAP subtype ($p=0.009$) and the LUM+ FAP subtype ($p=0.05$) (Rubenstein, et al., 2020; Subramanian, et al., 2005).

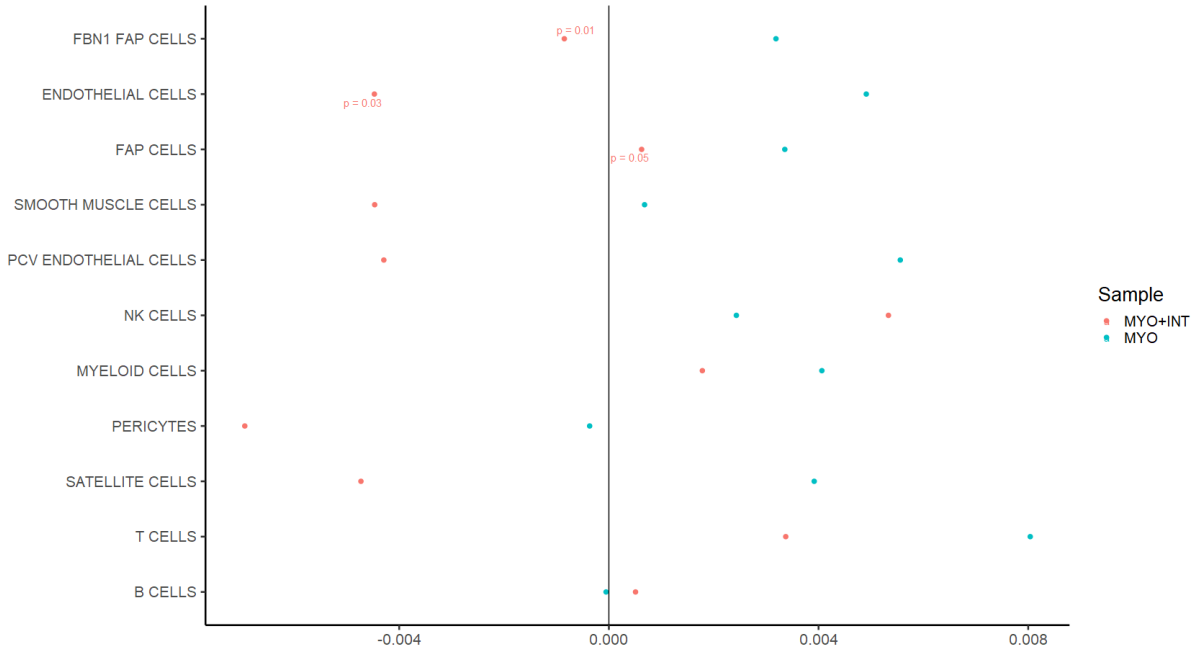

Figure 12 Over-representation analysis of skeletal muscle cell specific genes in the MYO and MYO+INT cell populations *(Rubenstein, et al., 2020; Subramanian, et al., 2005)*. X-axis depicts the mean ΔM across all DMPs in all the genes associated to the individual skeletal muscle subpopulation, indicating the overall direction and magnitude of DNA methylation change following RT.

6.0 Discussion

The present study aimed to investigate the cell-population specific similarities and differences in genome-wide DNA methylation between isolated myonuclei (MYO) and all nuclei derived from whole human skeletal muscle tissue (MYO+INT) following 7 weeks of resistance training. Firstly, all participants significantly increased their lower limb lean mass (7.9±3.1%) and VL & RF CSA of the biopsied leg (VL 18.2±5.7%, RF 15.6±9.1%) demonstrating the effectiveness of the implemented training program for inducing hypertrophy. Interestingly, while training volume load increased significantly, the isometric knee extension and flexion did not increase significantly following RT. This observation is in line with a previous study employing the same training program, where participant lean mass increased but not isometric strength following 7 weeks of RT (Seaborne R. A., et al., 2018), and similar observations where high volume RT led to superior hypertrophy but inferior strength gains compared to high load RT (Giessing, Eichmann, Steele, & Fisher, 2016).

6.1 main findings

The present study identified a substantial cell population specific differential DNA methylation in untrained and in trained human skeletal muscle. Of the ~804,000 CpG probes analyzed, 223,352 probes at baseline and 232,035 probes after RT exhibited differential methylation in MYO vs. MYO+INT cell populations. Furthermore, a relatively larger proportion of these probes were more hypomethylated in MYO vs. MYO+INT, which increased slightly from 56.2% at baseline (125,610/223,352) to 58.3% after RT (135,277/232,035). Indicating that the differing cell population specific DNA methylation diverges even further in trained vs. un-trained muscle. In addition, MYO+INT (20,543 DMPs post vs. baseline) and MYO (27,599 DMPs post vs. baseline) shared 901 DMPs, of which 548 DMPs had the same directionality between the cell populations after 7 weeks of RT. While there was some overlap between MYO and MYO + INT after training, there were clearly unique responses in methylation attributed to the myonuclei cell population, in line with our initial hypothesis. Although the myonuclear specific DNA methylation changes are incorporated in the whole tissue (MYO+INT) methylome, distinct contribution of hypo or hypermethylation from the MYO component may be masked by cell specific differential methylation originating from the interstitial cells detected in the MYO+INT samples. Despite previous research demonstrating cell population-specific DNA methylation changes in human blood (Reinius, et al., 2012) and in rat muscle (Wen, et al., 2021; Murach, Dungan, von Walden, & Wen, 2022), this is the first study to report cell population-specific DNA methylation profiles in untrained human skeletal muscle and post resistance training. Traditionally, in epigenome-wide association studies skeletal muscle has often been treated as a homogenous tissue in terms of its response to exercise, with little consideration given to the distinct cell populations within it (Barrès, et al., 2012; Begue, Raue, Jemiolo, & Trappe, 2017; Gorski, et al., 2022; Michaels, et al., 2013; Seaborne R. A., et al., 2018). However, the present findings underscore the need to account for the heterogeneity of skeletal muscle in interpreting epigenetic adaptations to exercise. The observed differences between MYO and MYO+INT highlight the importance of delineating the epigenetic responses of different cell populations within muscle tissue to understand, more accurately, the molecular mechanisms driving SkM adaptation to exercise.

One of the key findings in the present study is the identification of some distinct methylation signatures in the myonuclei (MYO) compared to the whole tissue (MYO+INT). When looking at the global methylation pattern following RT, we observed a predominantly hypomethylated response of 51.3% and 61.1% across all DMPs in both MYO+INT and MYO respectively (Figure. 7A), in line with previous studies (Seaborne R. A., et al., 2018; Sexton, et al., 2023; Blocquiaux, et al., 2020; Blocquiaux, et al., 2021). There were a greater proportion of hypomethylated DMPs within N_shelf, N_shore, Open-Sea, S-shelf and S_shores regions within the MYO versus the MYO+INT population (Figure 7C-D). However, when focusing on DMPs in CpG islands within promoter regions (Figure 7E), a greater prevalence of hypomethylation in MYO+INT (54.7%) and hypermethylation in MYO (70.7%) was observed, similar to that observed in myonuclei isolated from trained rodent muscle (Wen, et al., 2021). Indeed, recent work demonstrated larger promoter hypermethylation in myonuclei while interstitial nuclei were biased towards promoter hypomethylation (Wen, et al., 2021). However, the present study is the first to report such distinct epigenetic profiles across different cell populations in human muscle after resistance training. Thus, the unique methylation signature observed in myonuclei across studies that have utilized different species and training protocols may further depict the specialized functions of muscle versus non-muscle cells in response to mechanical and metabolic stimuli (Mukund & Subramaniam, 2019; Egan & Sharples, 2023).

6.2 A short discussion on specific DMPs and DMGs

A recent review-paper by Turner et al. (2019) identified multiple differentially expressed genes (DEGs) that were differentially methylated in one or more CpG cites following acute and chronic RT. Thus, indicating that differential methylation of individual probes can potentially affect the specific gene expression (Turner, Seaborne, & Sharples, 2019). Therefore, as the differential methylation of individual probes might be biologically relevant, the present study identified the most differentially methylated probes in the MYO+INT cell population, and compared the differential methylation with the MYO cell population following RT. Instead of merely using a p-value cutoff, we considered the relative DNA methylation change in post vs. baseline by filtering MYO+INT DMPs for $p < 0.0001$, or M-value change > 0.8. A p-value cutoff only approach would bias the analysis towards smaller DNA methylation changes following

RT, that were more consistent across participants. Equally interesting are the CpG probes that observed large absolute DNA methylation change, measured as M-value change, which were associated with higher variability and thus p values over 0.0001 but still within the 0.05 threshold (Figure 8). This analysis identified 40 most significant DMPs following RT, 19 hypomethylated and 21 hypermethylated. Interestingly, none of these 40 DMPs were significant DMPs in the MYO cell population following RT, however 22/40 had a tendency towards hypomethylation in MYO relative to MYO+INT. Although the interstitial cell population methylome was not directly assessed in the present study, it can be inferred from the observed DNA methylome differences between the myonuclear (MYO) and whole tissue (MYO+INT) cell populations. Given that the MYO methylome is a component of the MYO+INT methylome, the differential methylation observed between these two samples is likely reflective of the methylation patterns within the interstitial cell population. Therefore, of particular interest are the 8/40 DMPs that were hypomethylated in MYO+INT with a tendency towards hypermethylation in the MYO cell population, which suggests a potentially important role of these genes in interstitial cell adaptation to RT. These differentially methylated genes (DMGs) include three cell cycle and gene expression related genes (CCND1 - cell cycle progression; NBN - DNA repair; POLR1C – RNA polymerase I and III subunit 3), which is interesting as myonuclei are taught to be terminally differentiated (Holtzer, Marshall, & Finick, 1957). Thus, indicating a potential role of DNA methylation in regulation of genes involved in interstitial cell proliferation following RT. However, a recent study was able to identify myonuclear endoreplication in a SC ablation model (Borowik, et al., 2023), therefore not excluding the previously mentioned genes from playing a role in RT mediated adaptation within the myonuclei cell population. Additionally, the cytokine CXCL2 involved in inflammatory response was identified as one of the DMGs hypomethylated in MYO+INT with a tendency towards hypermethylation in MYO, suggesting potential heightened transcriptional readiness in the interstitial cell population. Cytokines are involved in the immune response in skeletal muscle following muscle damaging RT, and lead to the recruitment of immune cells to the site of damage, thus aiding in repair (Paulsen, Mikkelsen, Raastad, & Peake, 2012). However, gene expression data is required in order to confirm the changes in methylation are associated with alterations of expression in the direction hypothesized above.

Using the same criteria as for the identification of the most differentially methylated CpG probes in MYO+INT, we identified 41 CpGs with a $p < 0.0001$ or a M-value change over 0.8. Interestingly, 20/41 DMPs were hypomethylated following RT (Figure 9), none of which were significant DMPs in the MYO+INT cell population. Although none of these probes were DMPs in the MYO+INT cell population, identifying which of these were hypomethylated in MYO with a tendency towards hypermethylation in MYO+INT could potentially identify myonuclei specific DMGs. In MYO, 10/41 most differentially methylated probes were hypomethylated in MYO following RT, with a tendency toward hypermethylation in MYO+INT. Some of the interesting genes include; SMAD9 involved in signal pathways regulating pluripotency of stem cells and TGF-β and BMP signaling, where inhibition of BMP signaling in mice leads to muscle atrophy (Kanehisa & Goto, 2000; Sartori, et al., 2013), MAD1L1 which together with MAD2 forms the mitotic checkpoint complex that maintains chromosomal stability until the onset of anaphase, where the sister chromatids are pulled towards opposite ends of the cell (Luo, Ahmad, & Liu, 2018), FUBP1 is a master regulator of transcription, translation and RNA splicing (Debaize & Troadec, 2019), and is a key regulator of c-MYC gene expression which in turn regulated 10-15% of genes in the human genome (Avigan, Strober, & Levens, 1990), BANP forms an inhibitory complex with MDM2 that negatively regulates p53 a negative regulator of growth through regulation of genes involved in differentiation, cell cycle, apoptosis, gene amplification, DNA recombination, and cellular senescence (Pavithra, et al., 2009), and STRADA, a pseudo-kinase which forms a complex with MO25 and LKB1, a primary upstream kinase and thus activator of AMPK signaling (Kjøbsted, et al., 2018). As these genes were exclusively hypomethylated in myonuclei following RT, it is interesting that cell cycle related genes have a potentially increased transcriptional readiness, as myonuclei are taught to be terminally differentiated (Holtzer, Marshall, & Finick, 1957). However, a recent study found that myonuclei are not post-mitotic and a small fraction of myonuclei (1-3%) are able to replicate through endoreplication (Borowik, et al., 2023), which might propose a role of these genes in myonuclei following RT. Taken together, the theoretical roles of FUBP1, BANP and STRADA align with the resistance trained skeletal muscle phenotype, through their roles in maintaining energy homeostasis (Kjøbsted, et al., 2018), decreased negative regulation through p53 inhibition (Pavithra, et al., 2009), and increased transcription through potentially

increased c-MYC expression (Debaize & Troadec, 2019; Avigan, Strober, & Levens, 1990). However, gene expression data is required to confirm that the changes in methylation are associated with alterations of expression in the direction hypothesized above.

6.3 Differentially methylated pathways in myonuclei (MYO) and whole muscle tissue (MYO+INT) following resistance training

Focusing on gene pathways rather than solely on individual probes and genes provides a broader picture of the biological implications of differential DNA methylation, and as such is a key target for elucidating the role of differential methylation in MYO vs. MYO+INT samples following RT (Kanehisa & Goto, 2000). At the pathway level, we identified a set of differentially methylated KEGG pathways following RT, of which only 14 were shared in MYO and in MYO+INT samples. Of the identified pathways that were significantly over-represented in both MYO and MYO+INT samples post-RT, six (Lysine degradation; Cell cycle; Oxytocin signaling pathway; Endocrine and other factor-regulated calcium reabsorption; Carbohydrate digestion and absorption; Transcriptional misregulation in cancer) displayed opposite directionality of methylation changes. The biological relevance of these distinct methylation patterns in MYO and MYO+INT within these pathways is interesting, as they are involved in a multitude of cellular processes. For instance, the Cell cycle pathway is crucial for cell proliferation, a key aspect of muscle hypertrophy following resistance training, such as proliferation of satellite cells and other interstitial cell populations aiding in the remodeling of the extracellular matrix (Loreti & Sacco, 2022; Brightwell, et al., 2022). Interestingly, the observed myonuclear hypermethylation compared with hypomethylation in MYO+INT of the Cell cycle pathway in the present study might suggest a cell population specific epigenetic regulatory mechanism, potentially regulating cell proliferation in a population specific manner following RT. This is relevant for adaptations to chronic RT as, for example, satellite cells (SC) have been shown to play a role in facilitating long term hypertrophy of muscle fibers, likely through fusion and myonuclear accretion, however this is still debated in human skeletal muscle (Paulsen, Mikkelsen, Raastad, & Peake, 2012; Gundersen, 2016; Bagley, Denes, McCarthy, Wang, & Murach, 2023; Sharples & Turner, Skeletal Muscle Memory, 2023). Activation and proliferation of SC is essential to maintain the SC pool, as a reduction would diminish the regenerative

potential and thus blunt the adaptive response in skeletal muscle following RT (Schmidt, Schüler, Hütter, von Eyss, & von Maltzahn, 2019; Sambasivan, et al., 2011; Sharples & Turner, Skeletal Muscle Memory, 2023). With the current limited literature on epigenetic regulation of individual cell populations in skeletal muscle, we observe varied findings of the cell cycle epigenome. Using ATAC-seq to identify histone modification, the cell cycle pathway was not significant in fast- or slow phenotype rodent muscle (Bengtsen, et al., 2021). Following progressive weighted wheel running, cell cycle promoter hypomethylation was identified in rodent myonuclei (Wen, et al., 2021), however, cell cycle methylome was not significant between resident vs. newly acquired myonuclei (Murach, Dungan, von Walden, & Wen, 2022). When looking at whole tissue DNA methylome (equivalent to MYO+INT in the present study), Blocquiaux et al. (2021) and Seaborne et al. (2018) did not identify differential methylation of the cell cycle pathway following RT or recurrent RT. Conversely, Gorski et al. (2022) identified cell cycle hypomethylation after aerobic training in cancer survivors relative to healthy age-matched participants. Taken together, the contemporary literature together with the present study, indicate a potential role of epigenetic regulation of the cell cycle pathway of individual cell populations in skeletal muscle. However, further investigations are required, as these studies employed varying training modalities (resistance training vs. aerobic training), two different epigenetic markers (histone modification vs. DNA methylation), different species (human vs. rodent), and different analysis (all DMPs vs. promoter associated DMPs).

Another interesting pathway is the NF-κβ signaling pathway, which is a family of transcription factors that are activated by TNF-α, an inflammatory cytokine that when acutely elevated induces SC proliferation, and conversely chronically elevated induces SkM atrophy (Sharples, et al., 2016; Verhelst, Carpentier, & Beyaert, 2011). Interestingly, one TNF-α promoter associated DMP was identified as hypermethylated exclusively in the MYO cell population following RT, indicating a potential epigenetic transcriptional suppression in myonuclei. Possibly leading to a lower TNF-α gene expression in myonuclei at rest/chronically. This is interesting as acute but transiently increased intramuscular TNF-α promotes SC proliferation, however, chronic intramuscular increases lead to impaired differentiation and fusion (Foulstone, Huser, Crown, Holly, & Stewart, 2004; Sharples, et al., 2016). Even slightly elevated chronic TNF-α levels in muscle are associated with age related degradation, and

reduction/blocking of TNF-α has been shown prevent sarcopenia (Sciorati, et al., 2020; Wu, et al., 2023). However, gene expression data is required to confirm that the changes in methylation are associated with alterations of expression in the direction hypothesized above.

While TNF-α was exclusively hypermethylated in MYO following RT, the NF-κβ signaling pathway was significantly hypermethylated exclusively in the MYO+INT cell populations. The sparce literature on skeletal muscle cell specific NF-kB signaling provides some insight into its epigenetic regulation, however previous studies have only looked at rodent myonuclei. Acutely, the TNF-α NF-κβ signaling pathway was hypomethylated following three days of overload by synergist ablation (Von Walden, et al., 2020), in contrast to the present study where TNF-α NF-κβ signaling pathway was not significantly differentially methylated. Chronically, the NF-κβ signaling pathway was hypomethylated in promoter associated DMPs in myonuclei following progressive weighted wheel running (Wen, et al., 2021), in contrast to the present study where NF-κβ signaling was hypermethylated exclusively in the MYO+INT cell populations. Although, the methodological difference, such as species, muscle group, and training protocol between the present study and previous studies might explain this observed discrepancy (Wen, et al., 2021; Von Walden, et al., 2020). NF-κβ signaling has been implicated as a key regulator of skeletal muscle adaptation to exercise, amongst others aiding in tissue remodeling, SC proliferation and increased oxidative capacity (Kramer & Goodyear, 2007; Sharples, Stewart, & Seaborne, 2016; Foulstone, Huser, Crown, Holly, & Stewart, 2004). However, the role of epigenetic regulation of NF-κβ signaling related genes in the different cell populations in skeletal muscle tissue following RT has not been fully elucidated.

6.3.1 Growth and energy turnover related KEGG pathways are differentially methylated in myonuclei (MYO) vs. whole skeletal muscle tissue (MYO+INT)

To further elucidate methylation changes following RT, we turn our focus to the broader methylation patterns across RT related gene sets and pathways. Interestingly, the growth related PI3K/Akt pathway was exclusively over-represented in the MYO+INT only cell population. Hypomethylation of the PI3K/Akt signaling pathway following RT may have several beneficial effects on muscle function and adaptation, including enhanced protein synthesis, improved glucose metabolism, and improved muscle cell

survival (Schiaffino & Mammucari, 2011). The over-representation of the PI3K/Akt pathway in MYO+INT may suggest a heightened transcriptional readiness of related genes in the interstitial cells relative to myonuclei alone. However, our analysis identified 202/347 and 211/347 DMGs within the PI3K/Akt pathway in MYO+INT and MYO samples, respectively. Suggesting a relative importance of DNA methylation in PI3K/Akt pathway related genes in the myonuclear and interstitial cell populations, promoting adaptation to resistance training.

The insulin pathway, another key player in muscle growth and metabolism, showed a tendency towards significant over-representation in MYO (MYO $p = 0.07$, MYO+INT $p = 0.26$). Although this trend did not reach statistical significance, the distinct hypomethylation trend seen in MYO (mean ΔM-value = -0.008) in contrast with the slight hypermethylation trend in MYO+INT (mean ΔM-value = 0.002) may indicate differential methylation in myonuclei vs. interstitial cells. Wen et al. (2021) recently identified hypermethylated promoters in Insulin signaling in interstitial cells following progressive weighted wheel running in rodents, when looking at interstitial cells alone. Therefore, by looking at the difference in the methylation profile of insulin signaling in the MYO and MYO+INT samples, the tendency towards hypermethylation in MYO+INT indicates a hypermethylated profile in human skeletal muscle interstitial cells following RT, in line with recent rodent data (Wen, et al., 2021).

In addition, we identified that the AMPK signaling pathway was significantly over-represented and predominantly hypomethylated in the MYO cell population, suggesting potential increased gene transcription and AMPK activity. However, cell signaling and gene expression analysis would have to be undertaken to confirm this. The over-representation analysis identified 84/120 DMGs in myonuclei in the AMPK pathway. This could lead to beneficial adaptations such as enhanced glucose uptake and fatty acid oxidation. Additionally, increased AMPK related gene transcription could potentially aid in regulation of MPS/MPB through crosstalk between AMPK and mTOR pathways, modulating skeletal muscle adaptation to RT (Zhao, et al., 2017; Kjøbsted, et al., 2018). As a key regulator of energy homeostasis, the AMPK pathway has largely been investigated in the presence of aerobic exercise (Egan & Sharples, 2023; Grahame, 2004). While Ahtiainen et al. (2015) showed that AMPK pathway activation

in resistance training might be volume dependent, in line with our data suggesting AMPK as a potentially epigenetically regulated pathway following high volume RT.

6.3.2 Canonical Wnt signaling pathway is differentially methylated in MYO vs. MYO+INT

Interestingly, it seems that the DMGs and differential methylation between MYO and MYO+INT is centered around the canonical Wnt pathway, largely around the scaffold complex related to upstream and downstream regulation of the activity and effect of β-catenin. Previous studies in cardiac muscle have implicated Wnt/β-catenin in the regulation of cardiomyocyte growth, and in the growth of skeletal muscle following mechanical overload (Armstrong & Esser, 2005). To our knowledge, no studies have looked at the cell-population specific responses of Wnt pathway related genes following exercise. However, in line with a recent study in mouse muscle (Wen, et al., 2021), our data suggests a differential role of Wnt signaling in human myonuclei and interstitial cells, in agreement with our secondary hypothesis. The physiological significance of the differential methylation identified in the canonical Wnt pathway in mature skeletal muscle is still unclear, and we suggest that future studies should focus on cell population specific transcriptomics and proteomics of the DMGs identified in this study.

Interestingly, the pattern of hypo- and hyper methylation in MYO, with the hypomethylation of Frizzled/FZD8, DVL3 and hypermethylation of FRAT2, CTBP1 and CHD8 could perhaps collectively inhibit the downstream targets of canonical Wnt signaling, leading to an inhibition and reduced expression of cell cycle related factors/genes (Leal, et al., 2011). Conversely, the opposite pattern is observed in MYO+INT, with hypermethylation of Frazzled/FZD8, DVL3 and FRAT2, and a hypomethylation of FRAT2 and CTBP1, that could alternatively lead to an increased β-catenin signaling leading to increased activity and expression of cell cycle related factors/genes (Leal, et al., 2011; Kanehisa & Goto, 2000; Kanehisa M. , 2019). However, gene expression and protein activity and abundance of β-catenin related signaling following exercise requires further investigation.

6.4 Resistance training induced cellular flux and cell population specific differential methylation

The epigenetic regulation of individual genes is highly cell-specific, and previous studies in complex tissues have concluded that accounting for cell-type heterogeneity is critical in epigenome wide association studies (Michaels, et al., 2013; Jaffe & Irizarry, 2014; Cheow, et al., 2016). Complex tissues are therefore prone to false positive and false negatives, when interpreting epigenome wide results to one specific cell population. Previous studies in skeletal muscle have addressed this issue by mechanically isolating single fibers before analyzing the transcriptome and methylome, thereby reducing the non-myogenic signal (Chemello, et al., 2011; Begue, Raue, Jemiolo, & Trappe, 2017). Single cell and single nuclear omics are a novel field that has just recently ventured into the field of exercise science, however mainly focusing on transcriptomics (Lovrić, et al., 2021; Dos Santos, et al., 2020; Soule, et al., 2023). A recent study in isolated myonuclei was able to show a more detailed myonuclear specific epigenetic profile, which affected the signal from gene specific loci and functional ontological analysis, increasing agreement with muscle subtype specific function (Bengtsen, et al., 2021). Interestingly, we found two FAP subtypes, FBN1+ and LUM+, and Endothelial cells to be exclusively over-represented in the MYO+INT cell population. This finding raises new questions about the specific roles these cells may play in the adaptation of muscle to resistance training. Suggesting these skeletal muscle sub-populations as interesting targets in future EWAS, deconvoluting cell specific epigenetic changes and their role in skeletal muscle adaptation to resistance training.

Taken together, our data provides interesting insight on the intricate relationship between skeletal muscle adaptation to chronic resistance training, DNA methylation changes, and cellular dynamics. A key observation in the present study was the differential DNA methylation profiles in whole muscle tissue (MYO+INT) compared to myonuclei (MYO) alone, with an exclusive over-representation of the Leukocyte transendothelial migration KEGG term in the MYO+INT cell population. This over-represented gene-set is linked with cellular migration, and may indicate a potential influx of leukocytes into the skeletal muscle tissue following chronic RT, in agreement with our tertiary hypothesis. Leukocyte infiltration is a well-documented response to

muscle damage (Paulsen, Mikkelsen, Raastad, & Peake, 2012; Paulsen, et al., 2010; Rigamonti, Zordan, Sciorai, Rovere-Querini, & Brunelli, 2014) and can significantly influence the local tissue environment, including the epigenetic landscape. The transendothelial migration of these cells represents a key phase of the muscle damage induced inflammatory response, allowing leukocytes to exit the vasculature and penetrate the surrounding tissue. While this process is involved in muscle repair and adaptation (Paulsen, Mikkelsen, Raastad, & Peake, 2012), our findings suggest that it may introduce a confounding factor when interpreting the methylation changes in whole muscle tissue. As such, an increase in intramuscular leukocyte population following resistance training could contribute to the DNA methylation profile of the MYO+INT cell population, causing it to diverge from that of the MYO only cell population. By isolating myonuclei from human skeletal muscle we were able to show that DMPs in MYO following RT were not over-represented in any other cell population. Furthermore, in agreement with the contemporary literature, we observed a clear difference in gene specific methylation loci and in the over representation of gene sets related to muscle function. Future research should strive to elucidate the cell specific gene expression regulatory mechanisms in skeletal muscle tissue, furthering our understanding of the molecular mechanisms underlying cell population specific exercise adaptations.

6.4 Limitations

A potential limitation in the present study is the relatively small sample size, which may limit the generalizability of the findings. Additionally, our study focused exclusively on the analysis of DNA methylation patterns and did not investigate other epigenetic marks, such as histone modifications or non-coding RNAs, which may also play important roles in regulating skeletal muscle gene expression (Egan & Sharples, 2023). Future studies should explore the interplay between different epigenetic marks in skeletal muscle tissue and their potential functional consequences.

In the present study, due to accessibility, cost and efficiency, MACS with the PCM1 antibody was chosen to isolate the myonuclear proportion from the whole tissue. Although MACS has been shown to be effective and reliable for isolating myonuclei (Bengtsen, et al., 2021; Winje, et al., 2018; Viggars, et al., 2023), FACS could potentially have provided us with a more accurate sorting of nuclei and provided a

count of the different nuclear proportions in the skeletal muscle tissue before and after RT (Sutermaster & Darling, 2019; Soule, et al., 2023; Lovrić, et al., 2021). Additionally, the choice of MACS limited the number of skeletal muscle tissue cellular subpopulations we were able to isolate from the tissue samples. Thus, limiting our comparison to MYO vs. MYO+INT, as opposed to Wen et al. (2021) that was able to directly compare MYO vs. INT in rodents following weighted wheel running. Although the difference in DNA methylation between MYO and MYO+INT theoretically is attributable to the interstitial cell populations, there is no way of computing this profile without knowing the specific cell population proportions in the given samples. Therefore, we recommend that future studies employ epigenomic profiling from FACS separated nuclei (Soule, et al., 2023), using reduced representation bisulfite sequencing (RRBS) or other methods which requires less DNA and provides greater genomic coverage than the Illumina EPIC array (Carmona, et al., 2017; Pidsely, et al., 2016; Begue, Raue, Jemiolo, & Trappe, 2017), to perform cell population specific epigenetic profiling of all subpopulations that have already been shown to have unique gene expression profiles (Lovrić, et al., 2021; Rubenstein, et al., 2020). Furthermore, a recent study identified differential DNA methylation profiles between fast/glycolytic and slow/oxidative muscle, indicating that individual skeletal muscle fibre-types potentially have unique epigenomic profiles (Bengtsen, et al., 2021; Begue, Raue, Jemiolo, & Trappe, 2017).

Additionally, there is the consideration of satellite cell (SC) proliferation and fusion with existing muscle fibers following RT. Although, the PCM1 antibody should specifically label myonuclei (Winje, et al., 2018), satellite cells have been shown to contain PCM1 at the centrosome poles, as opposed to the myonuclear envelope (Viggars, et al., 2023). This “miss”-labeling of satellite cells by PCM1 seems to increase in a mode and dose dependent manner, indicating a potential correlation with degree of muscle damage and regeneration (Viggars, et al., 2023). Although the present study employed traditional RT methods that typically induce minimal muscle damage (Paulsen, Mikkelsen, Raastad, & Peake, 2012), we cannot rule out the potential contamination of SC in the MYO cell proportions. To address this issue, we co-stained skeletal muscle cross sections of all participants before and after RT to identify potential “miss”-labeling. Unfortunately, the quantification of histological analysis was outside the time-constraint of the present thesis but will be included in the subsequent publication.

Moreover, the epigenetic profile of recently fused myonuclei may retain DNA methylation consistent with the SC niche, and therefore appear distinct from the resident myonuclei (Murach, Dungan, von Walden, & Wen, 2022). Murach et al. (2022) showed that DNA methylation profiles of resident myonuclei had increased transcriptional readiness for growth related genes, while SC derived myonuclei (recently fused) had increased transcriptional readiness for transcription factor, cell-cell signaling, and ribosomal biogenesis related genes (Murach, Dungan, von Walden, & Wen, 2022). Therefore, in the present study the SC derived myonuclei could potentially mask some of the cell population specific differential DNA methylation following RT, as they likely retained some of the SC-niche DNA methylation profile also contained in the MYO+INT cell population.

In addition, the methylation of individual CpGs can have different effects on gene expression, based on the CpGs location (Jayavelu, Jajodia, Mishra, & Hawkins, 2020; Jones, 2012). This was demonstrated in a recent study of DNA methylation and gene expression patterns in the cancer genome atlas, where the majority of probes display the expected correlation consistent with hypermethylation induced gene silencing. However, the same study identified a significant proportion of genes with opposite or mixed correlations depending on the location of the CpG probe (Spainhour, Seo Lim, V Yi, & Qiu, 2019). Additionally, when overlapping methylome and transcriptome of skeletal muscle, only ~40% of DEGs were associated with differential methylation, and a larger correlation was observed between hypomethylation and increased gene expression than hypermethylation and reduced gene expression (Turner, Seaborne, & Sharples, 2019). Therefore, a standard good practice is always to confirm the gene specific methylation pattern with gene expression (Michaels, et al., 2013), to identify the methylation regulated differentially expressed genes (MeDEG). Unfortunately, within the time constraints of the present master's project, we ran out of time to perform rt-qPCR or RNAseq on the RNA that was isolated from the skeletal muscle tissue. Therefore, whether the differential methylation identified in the present study led to alterations in gene expression remains to be determined.

Same as with gene expression, we did not have time to perform extensive histological analysis to check cell-population shift or changes in myonuclear proportion, fiber size and fiber type shift, immune cell infiltration etc. Therefore, ORA of skeletal muscle cell-

population specific genes was our best option to infer cell-population specific changes. Although this method has previously been used by others (Voisin, et al., 2023), to our knowledge no validation study has investigated if this method is able to detect confounding in EWAS by cell population specific gene expression and/or cell population proportion shifts.

7.0 Conclusion

The results presented in this thesis provide novel insights into the epigenetic landscape of human skeletal muscle tissue, with important implications for understanding the molecular mechanisms governing skeletal muscle adaptation to chronic resistance training. In line with previous DNA methylation studies in complex tissues (Reinius, et al., 2012), we conclude that interpretation of whole skeletal muscle tissue methylation profiles should begin to take account of cell nuclei specific alterations and that the differences between myonuclear and interstitial DNA methylation profiles resulting from varying myonuclear and interstitial cell proportions should be considered. We observed distinct DNA methylation signatures in MYO compared to MYO+INT, with a greater proportion of hypomethylated DMPs in MYO. However, when looking at CpG islands within gene promoter regions the MYO cell population had a predominantly hypermethylated profile. Furthermore, our pathway analysis revealed differentially methylated pathways in MYO and MYO+INT, highlighting the potential for cell-specific transcriptional regulation in response to RT. Interestingly, the canonical WNT/β-catenin pathway was hypermethylated in MYO and hypomethylated in MYO+INT, suggesting a potentially differential role in the myonuclei vs. interstitial cells following RT.

References

Ahtiainen, J. P., Walker, S., Silvennoinen, M., Kyröläinen, H., Nindl, B. C., Häkkinen, K., . . . Hulmi, J. J. (2015). Exercise type and volume alter signaling pathways regulating. *European Journal of Applied Physiology*. doi:https://doi.org/10.1007/s00421-015-3155-3

Aloisi, M., Mussini, M., & Schiffino, S. (1973). Activation of muscle nuclei in denervation and hypertrophy. *Basic Research in Myology*, 338-345.

Armstrong, D. D., & Esser, K. A. (2005). Wnt/beta-catenin signaling activates growth-control genes during overload-induced skeletal muscle hypertrophy. *American journal of physiology. Cell physiology*, C853-C859. doi:https://doi.org/10.1152/ajpcell.00093.2005

Avigan, M. I., Strober, B., & Levens, D. (1990). A far upstream element stimulates c-myc expression in undifferentiated leukemia cells. *Journal of biological chemistry*.

Baar, K., & Esser, K. (1999). Phosphorylation of p70S6kcorrelates with increased skeletal muscle mass following resistance exercise. *American journal of Physiology*, 120-127. doi:https://doi.org/10.1152/ajpcell.1999.276.1.c120

Bagley, J. R., Denes, L. T., McCarthy, J. J., Wang, E. T., & Murach, K. A. (2023). The myonuclear domain in adult skeletal muscle fibres: past, present and future. *Journal of Physiology*, 723-741. doi:https://doi.org/10.1113/JP283658

Barrès, R., Yan, J., Egan, B., Treebak, J. T., Rasmussen, M., Fritz, T., . . . Zierath, J. R. (2012). Acute exercise remodels promoter methylation in human skeletal muscle. *Cell Metabolism*. doi:https://doi.org/10.1016/j.cmet.2012.01.001

Begue, G., Raue, U., Jemiolo, B., & Trappe, S. (2017). DNA methylation assessment from human slow- and fast-twitch skeletal muscle fibers. *Journal of Applied Physiology*. doi:https://doi.org/10.1152/japplphysiol.00867.2016

Bengtsen, M., Winje, I. M., Eftestøl, E., Landskron, J., Sun, C., Nygård, K., . . . Gundersen, K. (2021). Comparing the epigenetic landscape in myonuclei purified with a PCM1 antibody from a fast/glycolytic and a slow/oxidative muscle. *PLOS Genetics*. doi:https://doi.org/10.1371/journal.pgen.1009907

Bjørnsen, T., Wernbom, M., Løvstad, A., Paulsen, G., D'Souza, R. F., Cameron-Smith, D., . . . Raastad, T. (2019). Delayed myonuclear addition, myofiber hypertrophy, and increases in strength with high-frequency low-load blood flow restricted training to volitional failure. *Journal of Applied Physiology*, 578-592. doi:https://doi.org/10.1152/japplphysiol.00397.2018

Blocquiaux, S., Gorski, T., Roie, E. V., Ramaekers, M., Thienen, R. V., Nielens, H., . . . Thomis, M. (2020). The effect of resistance training, detraining and retraining on muscle strength and power, myofibre size, satellite cells and myonuclei in older men. *Experimental Gerontology*. doi:https://doi.org/10.1016/j.exger.2020.110860

Blocquiaux, S., Ramaekers, M., Van Thienen, R., Nielens, H., Delecluse, C., De Bock, K., & Thomis, M. (2021). Recurrent training rejuvenates and enhances transcriptome and methylome responses in young and older human muscle. *JCSM Rapid Communications*, 10-32. doi:http://dx.doi.org/10.1002/rco2.52

Bodine, S. C., Stitt, T. N., Gonzalez, M., Kline, W. O., Stover, G. L., Bauerlein, R., . . . Yancopoulos, G. D. (2001). Akt/mTOR pathway is a crucial regulator of skeletal muscle hypertrophy and can prevent muscle atrophy in vivo. *Nature Cell Biology*, 1014-1019. doi:https://doi.org/10.1038/ncb1101-1014

Borowik, A. K., Davidyan, A., Peelor III, F. F., Voloviceva, E., Doidge, S. M., Bubak, M. P., . . . Miller, B. F. (2023). Skeletal Muscle Nuclei in Mice are not Post-mitotic. *Function*. doi:https://doi.org/10.1093/function/zqac059

Brightwell, C. R., Latham, C. M., Thomas, N. T., Keeble, A. R., Murach, K. A., & Fry, C. S. (2022). A glitch in the matrix: the pivotal role for extracellular matrix remodeling during. *Americal journal of physioogy. Cell Physiology*. doi:https://doi.org/10.1152/ajpcell.00200.2022

Bruusgaard, J. C., Johansen, I. B., Egner, I. M., Rana, Z. A., & Gundersen, K. (2010). Myonuclei acquired by overload exercise precede hypertrophy and are not lost on detraining. *Proceedings of the National Academy of Sciences*, 15111-15116. doi:https://doi.org/10.1073/pnas.0913935107

Burzyn, D., Kuswanto, W., Klodin, D., Shadrach, J. J., Cerletti, M., Jang, Y., . . . Mathis, D. (2013). A Special Population of Regulatory T Cells Potentiates

Muscle Repair. *Cell Press*, 1282-1295. doi:https://doi.org/10.1016/j.cell.2013.10.054

Carmona, J. J., Accomando, W. P., Binder, A. M., Hutchinson, J. N., Pantano, L., Izzi, B., . . . Michels, K. B. (2017). Empirical comparison of reduced representation bisulfite sequencing and Infinium BeadChip reproducibility and coverage of DNA methylation in humans. *NPJ Genomic Medicine*. doi:https://doi.org/10.1038%2Fs41525-017-0012-9

Chemello, F., Bean, C., Cancellara, P., Laveder, P., Reggiani, C., & Lanfranchi, G. (2011). Microgenomic Analysis in Skeletal Muscle: Expression Signatures of Individual Fast and Slow Myofibers. *PLOS ONE*. doi:https://doi.org/10.1371/journal.pone.0016807

Cheow, L., Courtois, E. T., Tan, Y., Viswanathan, R., Xing, Q., Tan, R. Z., . . . Burkholder, W. F. (2016). Single-cell multimodal profiling reveals cellular epigenetic heterogeneity. *Nature Methods*, 833836. doi:https://doi.org/10.1038/nmeth.3961

Christiansen, S., Andersen, J., Kampmann, M., Liu, J., Andersen, M., Tfelt-Hansen, J., & Morling, N. (2022). Reproducibility of the Infinium methylationEPIC BeadChip assay using low DNA amounts. *Epigenetics*. doi:https://doi.org/10.1080/15592294.2022.2051861

Crossland, H., Kazi, A. A., Lang, C. H., Timmons, J. A., Pierre, P., Wilkinson, D. J., . . . Atherton, P. J. (2013). Focal adhesion kinase is required for IGF-I-mediated growth of skeletal muscle cells via a TSC2/mTOR/S6K1-associated pathway. *American journal of physiology. Endocrinology and metabolism*, 183-193. doi:https://doi.org/10.1152/ajpendo.00541.2012

Dammermann, A., & Merdes, A. (2002). Assembly of centrosomal proteins and microtubule organization depends on PCM-1. *The Journal of Cell Biology*, 255-266. doi:https://doi.org/10.1083/jcb.200204023

Debaize, L., & Troadec, M.-B. (2019). The master regulator FUBP1: its emerging role in normal cell function and malignant development. *Cellular and Molecular Life Sciences*, 259-281. doi:https://doi.org/10.1007/s00018-018-2933-6

Dos Santos, M., Backer, S., Saintpierre, B., Izac, B., Andrieu, M., Leturneur, F., . . . Maire, P. (2020). Single-nucleus RNA-seq and FISH identify coordinated transcriptional activity in mammalian myofibers. *Nat Commun*. doi:https://doi.org/10.1038/s41467-020-18789-8

Drummond, M. J., Fry, C. S., Glynn, E. L., Dreyer, H. C., Dhanani, S., Timmerman, K. L., . . . Rasmussen, B. B. (2009). Rapamycin administration in humans blocks the contraction-induced increase in skeletal muscle protein synthesis. *The Journal of Physiology*, 1535-1546. doi:https://doi.org/10.1113/jphysiol.2008.163816

Du, P., Zhang, X., Huang, C.-C., Jafari, N., Kibbe, W. A., Hou, L., & Lin, S. (2010). Comparison of Beta-value and M-value methods for quantifying methylation levels by microarray analysis. *BMC Bioinformatics*. doi:http://dx.doi.org/10.1186/1471-2105-11-587

Egan, B., & Sharples, A. P. (2023). Molecular Responses to Acute Exercise and Their Relevance for Adaptations in Skeletal Muscle to Exercise Training. *Physiological reviews*. doi:https://doi.org/10.1152/physrev.00054.2021

Elabd, C., Cousin, W., Upadhyayula, P., Chen, R. Y., Chooljian, M. S., Li, J., . . . Conboy, I. M. (2014). Oxytocin is an age-specific circulating hormone that is necessary for muscle maintenance and regeneration. *Nature Communications*. doi:https://doi.org/10.1038/ncomms5082

Eremenko, K. (2018). *Confident data skills.* Kogan Page.

Figuiredo, V. C., & McCarthy, J. J. (2019). Regulation of Ribosome Biogenesis in Skeletal Muscle Hypertrophy. *Physiology*, 30-42. doi:https://doi.org/10.1152/physiol.00034.2018

Flück, M., Carson, J. A., Gordon, S. E., Ziemiecki, A., & Booth, F. W. (1999). Focal adhesion proteins FAK and paxillin increase in hypertrophied skeletal muscle. *Journal of Physiology. Cell Physiology*, 152-162. doi:https://doi.org/10.1152/ajpcell.1999.277.1.C152

Foulstone, E. J., Huser, C., Crown, A. L., Holly, J. M., & Stewart, C. E. (2004). Differential signalling mechanisms predisposing primary human skeletal

muscle cells to altered proliferation and differentiation: role of IGF-I and TNFa. *Experimental Cell Research*, 223-235. doi:https://doi.org/10.1016/j.yexcr.2003.10.034

Giessing, J., Eichmann, B., Steele, J., & Fisher, J. (2016). A comparison of low volume 'high-intensity-training' and high volume traditional resistance training methods on muscular performance, body composition, and subjective assessments of training. *Biology of Sport*, 241-249. doi:https://doi.org/10.5604%2F20831862.1201813

Girardi, F., & Le Grand, F. (2018). Wnt Signaling in Skeletal Muscle Development and Regeneration. In J. Larrain, & G. Olivares, *Progress in Molecular Biology and Translational Science* (pp. 157-179). Academic Press. doi:https://doi.org/10.1016/bs.pmbts.2017.11.026

Goldberg, A. L. (1967). Work-inced growth of skeletal muscle in normal and hypophysectomized rats. *American Journal of Physiology*, 1193-1198. doi:https://doi.org/10.1152/ajplegacy.1967.213.5.1193

Gorski, P., Raastad, T., Ullrich, M., Turner, D., Hallén, J., Salvari, S. I., . . . Sharples, A. P. (2022). Aerobic exercise training resets the human skeletal muscle methylome 10 years after breast cancer treatment and survival. *The FASEB Journal*. doi:https://doi.org/10.1096/fj.202201510RR

Grahame, H. D. (2004). AMP-Activated Protein Kinase: A Key System Mediating Metabolic Responses to Exercise. *Medicine & Science in Sports & Exercise*, 28-34. doi:https://doi.org/10.1249/01.mss.0000106171.38299.64

Gundersen, K. (2016). Muscle memory and a new cellular model for muscle atrophy and hypertrophy. *Journal of Experimental Biology*, 235-242. doi:https://doi.org/10.1242/jeb.124495

Hatsell, S., Rowlands, T., Hiremath, M., & Cowin, P. (2003). β-Catenin and Tcfs in Mammary Development and Cancer. *Journal of mammary gland biology and neoplasia*, 145-158. doi:https://doi.org/10.1023/a:1025944723047

Holtzer, H., Marshall, J., & Finick, H. (1957). An analysis of myogenesis by the use of fluorescent antimyosin. *The Journal of biophysical and biochemical cytology*, 705-724. doi:https://doi.org/10.1083/jcb.3.5.705

Hornberger, T. A., Chu, W. K., Hsuiung, J. W., Huang, S. A., & Chien, S. (2006). The role of phospholipase D and phosphatidic acid in the mechanical activation of mTOR signaling in skeletal muscle. *PNAS*, 4741-4746. doi:https://doi.org/10.1073/pnas.0600678103

Hughes, D. C., Turner, D. C., Baehr, L. M., Seaborne, R. A., Viggars, M., Jarvis, J. C., . . . Sharples, A. P. (2021). Knockdown of the E3 ubiquitin ligase UBR5 and its role in skeletal muscle anabolism. *American journal of physiology. Cell physiology*, 45-56. doi:https://doi.org/10.1152/ajpcell.00432.2020

Huxley, A. F. (1957). Muscle structure and Theories of Contraction. *Progress in Biophysics and Biophysical Chemistry, 7*, 255-318. doi:https://doi.org/10.1016/S0096-4174(18)30128-8

Inoki, K., & Guan, K.-L. (2022). Rag GTPases regulate cellular amino acid homeostasis. *PNAS*. doi:https://doi.org/10.1073/pnas.2200788119

Jaenisch, R., & Bird, A. (2003). Epigenetic regulation of gene expression: how the genome integrates intrinsic and environmental signals. *Nature Genetics*, 245-254. doi:https://doi.org/10.1038/ng1089

Jaffe, A. E., & Irizarry, R. A. (2014). Accounting for cellular heterogeneity is critical in epigenome-wide association studies. *Genome Biology*. doi:https://doi.org/10.1186/gb-2014-15-2-r31

Janssen, I., Heymsfield, S. B., Wang, Z., & Ross, R. (2000). Skeletal muscle mass and distribution in 468 men and women aged 18–88 yr. *Journal of Applied Physiology*, 81-88. doi:https://doi.org/10.1152/jappl.2000.89.1.81

Jayavelu, N. D., Jajodia, A., Mishra, A., & Hawkins, D. R. (2020). Candidate silencer elements for the human and mouse genomes. *Nature Communications*. doi:https://doi.org/10.1038/s41467-020-14853-5

Jones, P. A. (2012). Functions of DNA methylation: islands, start sites, gene bodies and beyond. *Nature Reviews Genetics*, 484-492. doi:https://doi.org/10.1038/nrg3230

Kanehisa, M. (2019). Toward understanding the origin and evolution of cellular organisms. *Protein science : a publication of the Protein Society*, 1947–1951. doi:https://doi.org/10.1002/pro.3715

Kanehisa, M., & Goto, S. (2000). KEGG: kyoto encyclopedia of genes and genomes. *Nucleic acids research*, 27-30. doi:https://doi.org/10.1093/nar/28.1.27

Kanehisa, M., Furumichi, M., Sato, Y., Kawashima, M., & Ishiguro-Watanabe, M. (2023). KEGG for taxonomy-based analysis of pathways and genomes. *Nucleic acids research*, 587-592. doi:https://doi.org/10.1093/nar/gkac963

Kim, E., & Guan, K.-L. (2009). RAG GTPases in nutrient-mediated TOR signaling pathway. *Cell Cycle*, 1014-1018. doi:https://doi.org/10.4161/cc.8.7.8124

Kjøbsted, R., Hingst, J. R., Fentz, J., Foretz, M., Sanz, M.-N., Pehmøller, C., . . . Lantier, L. (2018). AMPK in skeletal muscle function and metabolism. *The Faseb Journal*. doi:https://doi.org/10.1096/fj.201700442R

Kramer, H. F., & Goodyear, L. J. (2007). Exercise, MAPK, and NF-κB signaling in skeletal muscle. *Jpurnal of Applied Physiology*, 388-395. doi:https://doi.org/10.1152/japplphysiol.00085.2007

Kubo, A., & Tsukita, S. (2013). Non-membranous granular organelle consisting of PCM-1: subcellular distribution and cell-cycle-dependent assembly/disassembly. *Journal of Cell Science*, 919-928. doi:https://doi.org/10.1242/jcs.00282

Kühl, M., Sheldahl, L. C., Park, M., Miller, J. R., & Moon, R. T. (2000). The Wnt/Ca2+ pathway. *Trends in Genetics*, 279-283. doi:https://doi.org/10.1016/S0168-9525(00)02028-X

Leal, M. L., Lamas, M., Aoki, M. S., Ugrinowitsch, C., Ramos, M. S., Tricoli, V., & Moriscot, A. S. (2011). Effect of different resistance-training regimens on the WNT-signaling pathway. *European journal of Applied Physiology*, 2535-2545. doi:https://doi.org/10.1007/s00421-011-1874-7

Li, Y., Inoki, K., & Guan, K.-L. (2004). Biochemical and functional characterizations of small GTPase Rheb and TSC2 GAP activity. *Molecular and cellular biology*, 7965–7975. doi:https://doi.org/10.1128/mcb.24.18.7965-7975.2004

Loreti, M., & Sacco, A. (2022). The jam session between muscle stem cells and the extracellular matrix in the tissue environment. *npj Regenerative Medicine, 16*. doi:https://doi.org/10.1038/s41536-022-00204-z

Lovrić, A., Rassolie, A., Alam, S., Mandić, M., Saini, A., Altun, M., . . . Rullman, E. (2021). Single-cell sequencing deconvolutes cellular responses to exercise in human skeletal muscle. *Commun Biol*. doi:https://doi.org/10.1038/s42003-022-04088-z

Luo, W., Friedman, M. S., Shedden, K., Hankenson, K. D., & Woolf, P. J. (2009). GAGE: generally applicable gene set enrichment for pathway analysis. *BMC Bioinformatics*. doi:https://doi.org/10.1186/1471-2105-10-161

Luo, Y., Ahmad, E., & Liu, S.-T. (2018). MAD1: Kinetochore Receptors and Catalytic Mechanisms. *Frontiers in Cell and Developmental Biology*. doi:https://doi.org/10.3389/fcell.2018.00051

Maaser, M.-F., Turner, D. C., Gorski, P. P., Seaborne, R. A., Strauss, J. A., Shepherd, S. O., . . . Sharples, A. P. (2021). The Comparative Methylome and Transcriptome After Change of Direction Compared to Straight Line Running Exercise in Human Skeletal Muscle. *Frontiers in Physiology*. doi:https://doi.org/10.3389/fphys.2021.619447

MacIntyre, D. L., Reid, W. D., Lyster, D. M., & McKenzie, D. C. (2000). Different effects of strenuous eccentric exercise on the accumulation of neutrophils in muscle in women and men. *European Journal of Applied physiology*, 47-53. doi:https://doi.org/10.1007/pl00013796

Maksimovic, J., Phipson, B., & Oshlack, A. (2023, February 1). *A cross-package Bioconductor workflow for analysing methylation array data*. Retrieved from bioconductor.ord: https://www.bioconductor.org/packages/release/workflows/vignettes/methylationArrayAnalysis/inst/doc/methylationArrayAnalysis.html

McGee, S. L., & Hargreaves, M. (2019). Epigenetics and Exercise. *Trends in Endocrinology & Metabolism*. doi:https://doi.org/10.1016/j.tem.2019.06.002

Michaels, K. B., Binder, A. M., Dedeurwaerder, S., Epstein, C. B., Greally, J. M., Gut, I., . . . Irizarry, R. A. (2013). Recommendations for the design and analysis of epigenome-wide association studies. *Nature Methods*, 949-955. doi:https://doi.org/10.1038/nmeth.2632

Mukund, K., & Subramaniam, S. (2019). Skeletal muscle: a review of molecular structure and function, in health and disease. *WIREs Systems Biology and Medicine*. doi:https://doi.org/10.1002/wsbm.1462

Murach, K. A., Dungan, C. M., von Walden, F., & Wen, Y. (2022). Epigenetic evidence for distinct contributions of resident and acquired myonuclei during long-term exercise adaptation using timed in vivo myonuclear labeling. *American Journal of Physioogy. Cell Physiology*, 86-93. doi:http://dx.doi.org/10.1152/ajpcell.00358.2021

Paulsen, G., Crameri, R., Brenestad, H. B., Fjeld, J. G., Mørkrid, L., Hallén, J., & Raastad, T. (2010). Time Course of Leukocyte Accumulation in Human Muscle after Eccentric Exercise. *Medicine and science in sports and exercise*, 75-85. doi:https://doi.org/10.1249/mss.0b013e3181ac7adb

Paulsen, G., Mikkelsen, U. R., Raastad, T., & Peake, J. M. (2012). Leucocytes, cytokines and satellite cells:what role do they play in muscle damage andregeneration following eccentric exercise? *Exercise immunology review*, 42-97.

Pavithra, L., Mukherjee, S., Sreenath, K., Kar, S., Sakaguchi, K., Roy, S., & Chattopadhyay, S. (2009). SMAR1 Forms a Ternary Complex with p53-MDM2 and Negatively Regulates p53-mediated Transcription. *Journal of Molecular Biology*, 691-702. doi:https://doi.org/10.1016/j.jmb.2009.03.033

Phipson, B., Maksimovic, J., & Oshlack, A. (2016). missMethyl: an R package for analyzing data from Illumina's HumanMethylation450 platform. *Bioinformatics*. doi:https://doi.org/10.1093/bioinformatics/btv560

Pidsely, R., Zotenkp, E., Peters, T. J., Lawrence, M. G., Risbridger, G. P., Molloy, P., . . . Clark, S. J. (2016). Critical evaluation of the Illumina MethylationEPIC BeadChip microarray for whole-genome DNA methylation profiling. *Genome Biology*. doi:https://doi.org/10.1186%2Fs13059-016-1066-1

Psilander, N., Eftestøl, E., Cumming, K. T., Juvkam, I., Ekblom, M. M., Sunding, K., . . . Gundersen, K. (2019). Effects of training, detraining, and retraining on strength, hypertrophy, and myonuclear number in human skeletal muscle. *Journal of Applied Physiology*. doi:https://doi.org/10.1152/japplphysiol.00917.2018

Purslow, P. P. (2010). Muscle fascia and force transmission. *Journal of Bodywork and movement Therapies*, 411-417. doi:https://doi.org/10.1016/j.jbmt.2010.01.005

Qi, L., & Teschendorff, A. E. (2022). Cell-type heterogeneity: Why we should adjust for it in epigenome and biomarker studies. *Clinical Epigenetics*. doi:https://doi.org/10.1186/s13148-022-01253-3

Reinius, L. E., Acevedo, N., Joerink, M., Pershagen, G., Dahlén, S.-E., Greco, D., . . . Kere, J. (2012). Differential DNA Methylation in Purified Human Blood Cells: Implications for Cell Lineage and Studies on Disease Susceptibility. *PLOS ONE*. doi:https://doi.org/10.1371/journal.pone.0041361

Rigamonti, E., Zordan, P., Sciorai, C., Rovere-Querini, P., & Brunelli, S. (2014). Macrophage Plasticity in Skeletal Muscle Repair. *BioMed Research International*. doi:https://doi.org/10.1155/2014/560629

Rubenstein, A. B., Smith, G. R., Raue, U., Begue, G., Minchev, K., Ruf-Zamojski, F., . . . Sealfon, S. C. (2020). Single-cell transcriptional profiles in human skeletal muscle. *Scientific Reports*. doi:https://doi.org/10.1038/s41598-019-57110-6

Sambasivan, R., Yao, R., Kissenpfenning, A., Van Wittenberghe, L., Paldi, A., Gayraud-Morel, B., . . . Galy, A. (2011). Pax7-expressing satellite cells are indispensable for adult skeletal muscle regeneration. *Development*. doi:https://doi.org/10.1242/dev.067587

Sandri, M. (2008). Signaling in Muscle Atrophy and Hypertrophy. *Physiology*, 160-170. doi:https://doi.org/10.1152/physiol.00041.2007

Sartori, R., Schirwis, E., Blaauw, B., Bortolanza, S., Zhao, J., Enzo, E., . . . Sandri, M. (2013). BMP signaling controls muscle mass. *Nature Genetics*, 1309-1318. doi:https://doi.org/10.1038/ng.2772

Schiaffino, S., & Mammucari, C. (2011). Regulation of skeletal muscle growth by the IGF1-Akt/PKB pathway: insights from genetic models. *Skeletal Muscle*. doi:https://doi.org/10.1186/2044-5040-1-4

Schmidt, M., Schüler, S. C., Hütter, S. S., von Eyss, B., & von Maltzahn, J. (2019). Adult stem cells at work: regenerating skeletal muscle. *Cellular and Molecular Life Sciences*, 2559-2570. doi:https://doi.org/10.1007/s00018-019-03093-6

Sciorati, C., Gamberale, R., Monno, A., Citterio, L., Lanzani, C., De Lorenzo, R., . . . Rovere-Querini, P. (2020). Pharmacological blockade of TNFα prevents sarcopenia and prolongs survival in aging mice. *Aging*, 23497-23508. doi:https://doi.org/10.18632%2Faging.202200

Seaborne, R. A., Hughes, D. C., Turner, D. C., Owens, D. J., Baehr, L. M., Gorski, P., . . . Sharples, A. P. (2019). UBR5 is a novel E3 ubiquitin ligase involved in skeletal muscle hypertrophy and recovery from atrophy. *The Journal of Physiology*, 3727-3749. doi:https://doi.org/10.1113/JP278073

Seaborne, R. A., Strauss, J., Cocks, M., Shepherd, S., O'Brien, T. D., van Someren, K. A., . . . Sharples, A. P. (2018). Human Skeletal Muscle Possesses an Epigenetic Memory of Hypertrophy. *Scientific Reports*. doi:https://doi.org/10.1038/s41598-018-20287-3

Seaborne, R. A., Strauss, J., Cocks, M., Shepherd, S., O'Brien, T., van Someren, K., . . . Sharples, A. (2018). Methylome of human skeletal muscle after acute & chronic resistance exercise training, detraining & retraining. *Scientific Data*. doi:https://doi.org/10.1038/sdata.2018.213

Sexton, C. L., Godwin, J. S., McIntosh, M. C., Ruple, B. A., Osburn, S. C., Hollingsworth, B. R., . . . Roberts, M. D. (2023). Skeletal Muscle DNA Methylation and mRNA Responses to a Bout of Higher versus Lower Load

Resistance Exercise in Previously Trained Men. *Cells*. doi:https://doi.org/10.3390/cells12020263

Sharples, A. P., & Turner, D. C. (2023). Skeletal Muscle Memory. *American Journal of Physiology. Cell Physiology*. doi:https://doi.org/10.1152/ajpcell.00099.2023

Sharples, A. P., Polydorou, I., Hughes, D. C., Owens, D. J., Hughes, T. M., & Stewart, C. E. (2016). Skeletal muscle cells possess a 'memory' of acute early life. *Biogerontology*, 603-617. doi:https://doi.org/10.1007/s10522-015-9604-x

Sharples, A. P., Stewart, C. E., & Seaborne, R. A. (2016). Does skeletal muscle have an 'epi'-memory? The role of epigenetics in nutritional programming, metabolic disease, aging and exercise. *Ageing Cell*, 603-616. doi:https://doi.org/10.1111/acel.12486

Snijders, T., Aussieker, T., Holwerda, A., Parise, G., van Loon, L. J., & Verdijk, L. B. (2020). The concept of skeletal muscle memory: Evidence from animal and human studies. *Acta Physiologica*. doi:https://doi.org/10.1111/apha.13465

Soule, T. G., Pontifex, C. S., Rosin, N., Joel, M., Lee, S., Nguyen, M., . . . Pfeffer, G. (2023). A protocol for single nucleus RNA-seq from frozen skeletal muscle. *Life Science Alliance*. doi:https://doi.org/10.26508/lsa.202201806

Spainhour, J. C., Seo Lim, H., V Yi, S., & Qiu, P. (2019). Correlation Patterns Between DNA Methylation and Gene Expression in The Cancer Genome Atlas. *Cancer informatics*. doi:https://doi.org/10.1177%2F1176935119828776

Spangenburg, E. E., Roith, D. L., Ward, C. W., & Bodine, S. C. (2008). A functional insuline-like growth factor receptor is not necessary for load-induced skeletal muscle hypertrophy. *Journal of Physiology*, 283-291. doi:https://doi.org/10.1113/jphysiol.2007.141507

Srsen, V., Fant, X., Heald, R., Rabouille, C., & Merdes, A. (2009). Centrosome proteins form an insoluble perinuclear matrix during muscle cell differentiation. *BMC Cell Biology*. doi:https://doi.org/10.1186/1471-2121-10-28

Stoothoff, W. H., Cho, J.-H., McDonald, R. P., & Johnson, G. V. (2004). FRAT-2 Preferentially Increases Glycogen Synthase Kinase 3β-mediated Phosphorylation of Primed Sites, Which Results in Enhanced Tau

Phosphorylation. *Journal of Biological Chemistry*. doi:https://doi.org/10.1074/jbc.M410061200

Subramanian, A., Tamayo, P., Mootha, V. K., Mukherjee, S., Ebert, B. L., Gillette, M. A., . . . Mesirov, J. P. (2005). Gene set enrichment analysis: A knowledge-based approach for interpreting genome-wide expression profiles. *PNAS*. doi:https://doi.org/10.1073/pnas.0506580102

Suter, M., Riek, U., Tuerk, R., Schlattner, U., Wallimann, T., & Dietbert, N. (2006). Dissecting the Role of 5′-AMP for Allosteric Stimulation, Activation, and Deactivation of AMP-activated Protein Kinase. *Journal of Biological Chemistry*. doi:https://doi.org/10.1074/jbc.M606357200

Sutermaster, B. A., & Darling, E. M. (2019). Considerations for high-yield, high-throughput cell enrichment: fluorescence versus magnetic sorting. *Scientific Reports*. doi:https://doi.org/10.1038/s41598-018-36698-1

Tipton, K. D., Ferrando, A. A., Phillips, S. M., Doyle Jr, D., & Wolfe, R. R. (1999). Postexercise net protein synthesis in human muscle from orally administered amino acids. *The American journal of physiology*, 628-634. doi:https://doi.org/10.1152/ajpendo.1999.276.4.e628

Turner, D. C., Seaborne, R. A., & Sharples, A. P. (2019). Comparative Transcriptome and Methylome Analysis in Human Skeletal Muscle Anabolism, Hypertrophy and Epigenetic Memory. *Scientific Reports*. doi:https://doi.org/10.1038/s41598-019-40787-0

Verhelst, K., Carpentier, I., & Beyaert, R. (2011). Regulation of TNF-induced NF-kB activation by different cytoplasmic. *Cytokine & growth factor reviews*, 277-286. doi:https://doi.org/10.1016/j.cytogfr.2011.11.002

Viggars, M. R., Owens, D., Stewart, C., Coirault, C., Mackey, A. L., & Jarvis, J. C. (2023). Investigating Pericentriolar Material-1 (PCM1) as a marker for skeletal muscle myonuclei : A cross-species and model PCM1 in skeletal muscle myonuclei and more. *American Journal of Physiology. Cell Physiology*, C85-C97. doi:https://doi.org/10.1152/ajpcell.00285.2022

Voisin, S., Seale, K., Jacques, M., Landen, S., Harvey, N. R., Haupt, L. M., . . . Eynon, N. (2023). Exercise is associated with younger methylome and transcriptome profiles in human skeletal muscle. *Aging Cell*. doi:https://doi.org/10.1111/acel.13859

Von Walden, F., Rea, M., Mobley, C., Fondufe-Mittendorf, Y., McCarthy, J. J., Peterson, C. A., & Murach, K. A. (2020). The myonuclear DNA methylome in response to an acute hypertrophic stimulus. *Epigenetics*. doi:https://doi.org/10.1080/15592294.2020.1755581

Wen, Y., Dungan, C. M., Mobley, C. B., Valentino, T., von Walden, F., & Murach, K. A. (2021). Nucleus Type-Specific DNA Methylomics Reveals Epigenetic "Memory" of Prior Adaptation in Skeletal Muscle. *Function*. doi:https://doi.org/10.1093/function/zqab038

Winje, I., Bengtsen, M., Eftestøl, E., Juvkam, I., Bruusgaard, J., & Gundersen, K. (2018). Specific labelling of myonuclei by an antibody against Pericentriolar material 1 (PCM1) on skeletal muscle tissue sections. *Acta Physiologica*, e13034. doi:https://doi.org/10.1111/apha.13034

Wu, J., Lin, S., Chen, W., Lian, G., Wu, W., Chen, A., . . . Xie, L. (2023). TNF-α contributes to sarcopenia through caspase-8/caspase-3/GSDME-mediated pyroptosis. *Cell Death Discovery*. doi:https://doi.org/10.1038/s41420-023-01365-6

Zhao, Y., Hu, X., Liu, Y., Dong, S., Wen, Z., He, W., . . . Shi, M. (2017). ROS signaling under metabolic stress: Cross-talk between AMPK and AKT pathway. *Molecular Cancer*. doi:https://doi.org/10.1186/s12943-017-0648-1